X-RAY AND GAMMA RAY ASTRONOMY DETECTORS

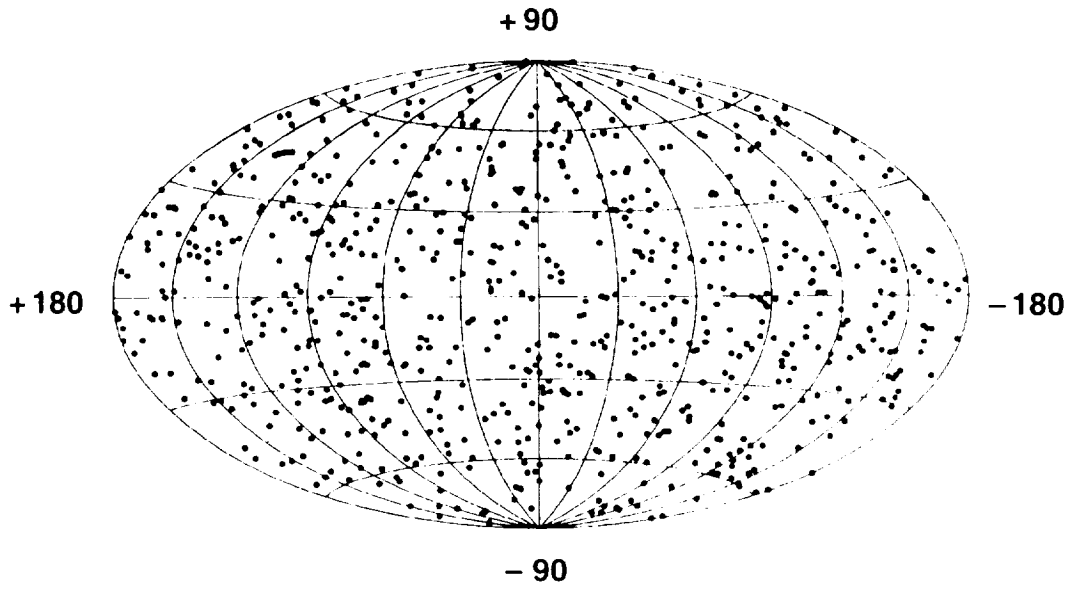

Cover: A sky map of 761 gamma ray bursts detected by the BATSE on the NASA Compton Gamma Ray Observatory in the first 29 months of operation. Burst locations are shown in galactic coordinates.

NASA SP-517

X-RAY AND GAMMA RAY ASTRONOMY DETECTORS

R. Decher

B.D. Ramsey

R. Austin

National Aeronautics and Space Administration
Scientific and Technical Information Program
Washington, D.C. 1994

Library of Congress Catalog Card Number 94-92211
For sale by the National Technical Information Service
Springfield, Virginia 22151

Contents

Preface

X-ray and gamma ray astronomy was made possible by the advent of space flight. Discovery and early observations of celestial x-rays and gamma rays, dating back almost 40 years, were first done with high altitude rockets, followed by Earth-orbiting satellites. Once it became possible to carry detectors above the Earth's atmosphere, a new view of the universe in the high-energy part of the electromagnetic spectrum evolved. Many of the detector concepts used for x-ray and gamma ray astronomy were derived from radiation measuring instruments used in atomic physics, nuclear physics, and other fields. However, these instruments, when used in x-ray and gamma ray astronomy, have to meet unique and demanding requirements related to their operation in space and the need to detect and measure extremely weak radiation fluxes from celestial x-ray and gamma ray sources. Their design for x-ray and gamma ray astronomy has, therefore, become a rather specialized and rapidly advancing field in which improved sensitivity, higher energy and spatial resolution, wider spectral coverage, and enhanced imaging capabilities are all sought.

This text is intended as an introduction to x-ray and gamma ray astronomy instruments. It provides an overview of detector design and technology and is aimed at scientists, engineers, and technical personnel and managers associated with this field. The discussion is limited to basic principles and design concepts and provides examples of applications in past, present, and future space flight missions. For more details and an in-depth treatment of the subject, the reader is referred to several available texts.[1-3,5-7] Portions of Chapters 3, 5, and 6 are reproduced with the kind permission of Space Science Reviews.

Rudolf Decher, Brian D. Ramsey, and Robert Austin

I. INTRODUCTION

X-rays and gamma rays are energetic photons covering the high-energy region of the electromagnetic spectrum above the ultraviolet (Figure 1) ranging from 10^2 eV to the highest energies observed (10^{13} eV). This radiation has extremely short wavelengths and is usually identified by energy. (For very low-energy x-rays, the wavelength λ as well as energy is used.) The photon energy E is expressed in electronvolts (eV), keV (10^3 eV), or MeV (10^6 eV). The energy is given by $E = h\nu$, where h is Planck's constant and $\nu = 1/\lambda$ is the frequency of the radiation. The conversion between wavelength λ (in Ångströms) and energy E (in keV) is given by $E = 12.4/\lambda$.

Traditionally, x-rays and gamma rays have been distinguished by the processes involved in their generation: photons generated by energy transitions in the inner electron shell of atoms are called x-rays, while photons generated by energy transitions in the nucleus of atoms are called gamma rays. In astrophysics the division between x-rays and gamma rays is based on a rather arbitrary energy limit which ranges from 30 keV to 511 keV, depending on personal preference. Photons with energies below this limit are considered x-rays and higher energy photons are called gamma rays. X-rays are often divided into soft x-rays (with energies below 10 keV) and hard x-rays (above 10 keV).

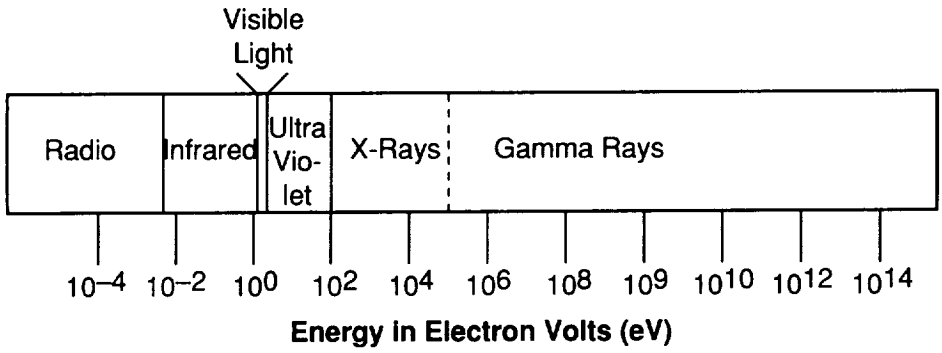

Fig. 1. The Electromagnetic spectrum.

X-Ray and Gamma Ray Astronomy Detectors

X-rays and gamma rays from astronomical sources are absorbed in the Earth's atmosphere and cannot be observed on the ground. Their detection and observations must be done from above the atmosphere using rockets or satellites. In addition, balloons which float at high altitudes can be used to observe radiation above 20 keV (lower energy radiation is absorbed in the atmospheric mass remaining above the balloon altitude). The first x-rays from the Sun were discovered in 1949 with detectors carried in a rocket. The first x-rays from a source outside the solar system were detected in 1962 using gas-filled detectors launched with an Aerobee sounding rocket, and the first high-energy gamma rays were detected by the Explorer XI satellite in 1961. Following these early discoveries, x-ray and gamma ray detectors were carried on many satellites. Several satellite observatories dedicated to x-ray and gamma ray astronomy and carrying a variety of detectors have been launched and new ones are under development for future space missions.

Many celestial objects including the Sun, other stars, hot gas clouds, supernova explosions and remnants (such as neutron stars and black holes), galaxies, and quasars emit x-rays and gamma rays.[2-4] The observed radiation may be continuous over a certain energy range and also may appear as discrete spectral lines. The radiation may be constant or variable with time or may occur as flashes of radiation at random times (e.g., gamma ray bursts). Analysis of the received radiation reveals information about the nature of the radiating source and the processes involved in the generation of x-rays and gamma rays. X-rays and gamma rays are emitted when high-energy charged particles and photons interact with each other, with other matter, and with magnetic fields. There are several mechanisms for the generation of x-rays and gamma rays[2-4] including acceleration of charged particles in the Coulomb field of an atom (Bremsstrahlung) or in magnetic fields (synchrotron radiation), electron-photon collisions (inverse Compton effect), electron-positron annihilation, and energy transitions in excited atomic nucleii. The latter two processes are also responsible for line radiation.

To detect x-ray or gamma ray photons requires their interaction with matter (in gaseous, liquid, or solid form) in the detector absorber. Photons interact with matter in many different ways depending on their energy and the type of material used in the detector.[2,3,5] Different interaction processes are utilized to design detectors which have optimum performance for a particular energy region and for the type of measurements intended. Among the various interaction processes, three are of im-

portance for detector design: the photoelectric effect, Compton scattering, and pair production.

A. PHOTOELECTRIC EFFECT

The photoelectric effect dominates at lower photon energies. In photoelectric interactions the incoming photon is absorbed in an atom and an electron (photoelectron) is ejected with a kinetic energy corresponding to the photon energy minus the electron's binding energy (Figure 2). The photoelectron loses energy by ionization and excitation of other atoms. The resulting charges are collected in the detector to generate a signal. The initial photon interaction generates an ionized atom with an electron vacancy which is filled by an electron from an outer shell or by a free electron from the absorber. This process generates additional electrons and photons which are either absorbed in the detector material or escape from the system. The photoelectric cross section (probability of occurrence) increases strongly with the atomic number (Z) of the material (it is approximately proportional to Z^5) which means, for example, photon absorption is much larger in lead (Z = 82) than in a lower Z material such as aluminum (Z = 13). The photoelectric cross section decreases with increasing energy E of the incident photon (it is proportional to $E^{-7/2}$).

B. COMPTON SCATTERING

Compton scattering is the dominant interaction for medium photon energies. In Compton interactions the incident photon collides with an electron usually in the outer shell of an atom where the electron binding energy is very small and can be neglected (Figure 2). The photon is scattered at an angle relative to the original direction of motion and it loses energy which is transferred to the electron. The scattered photon may experience further interactions (photoelectric or Compton scattering) and is either stopped in or escapes from the detector absorber material. The electron involved in the collision (recoil electron) is scattered at a different angle relative to the photon and loses its energy through ionization and excitation of other atoms until it is eventually stopped in the material. The amount of energy which can be transferred to the recoil electron depends on the scattering angle and the incident photon energy and may vary from

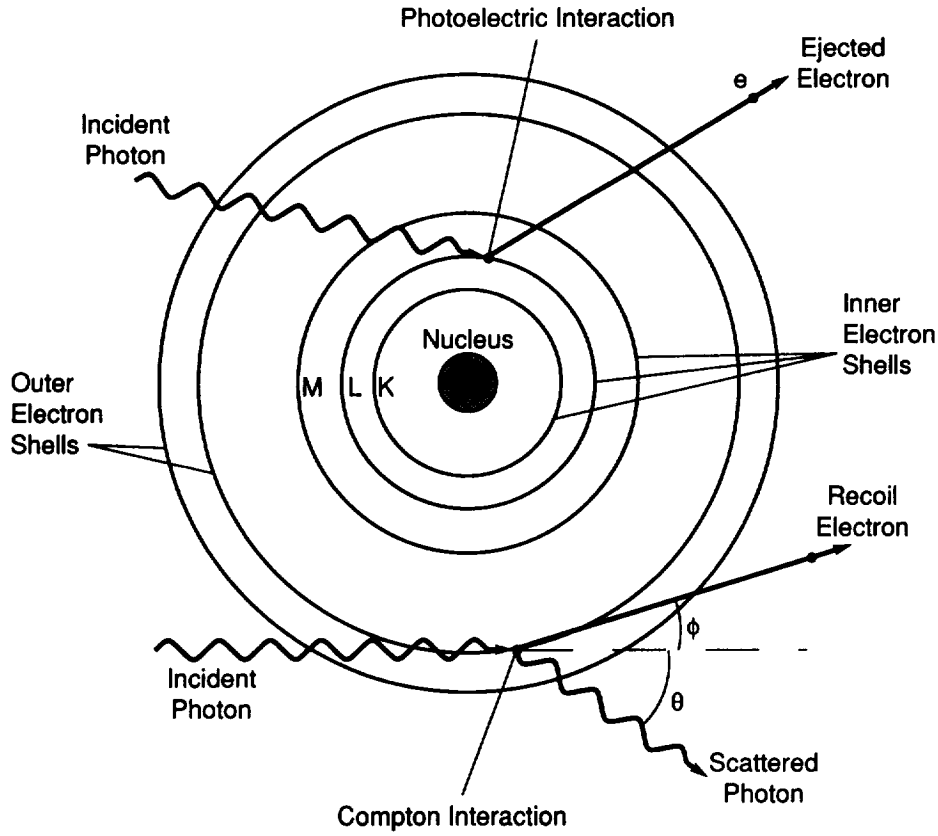

Fig. 2. Photoelectric and Compton interactions. In the photoelectric effect, the incident photon interacts with an inner shell electron which is ejected. In the Compton effect, the incident photon interacts with an outer shell electron. The photon and ejected electron are scattered at different angles.

zero to a large fraction of the incident photon energy. Maximum energy transfer occurs in a head-on collision but the photon still keeps some of its energy. The cross section for the Compton effect is proportional to the density of the material and inversely proportional to the energy of the incident photon.

C. PAIR PRODUCTION

At higher gamma ray energies (above several MeV) the pair production process becomes the dominant interaction. The incident gamma ray photon, which disappears in the process, is transformed into an electron-positron pair (Figure 3). This interaction requires the presence of the Coulomb field of an atomic nucleus. The incident photon must have an energy of at least 1.02 MeV to generate an electron-positron pair. (The energy equivalent of the rest mass of an electron or positron is 0.511 MeV each.) The incident photon energy in excess of the 1.02 MeV appears as kinetic energy of the electron and positron. Both particles will lose their energy through interactions with the detector absorber material. The positron is an unstable particle and after losing most of its kinetic energy it will combine with an electron. Both the electron and the positron disappear in this process which generates two 0.511 MeV photons (annihilation radiation). The probability of the pair production process increases with the atomic number Z of the absorber (it is proportional to Z^2) and with increasing energy of the incoming gamma ray photon.

The relative probabilities of the three photon interaction processes as a function of photon energy and atomic number (Z) of the detector material are indicated in Figure 4. The left curve represents equal probability for the photoelectric and Compton effect; the right curve corresponds to equal probability for Compton scattering and pair production interactions.

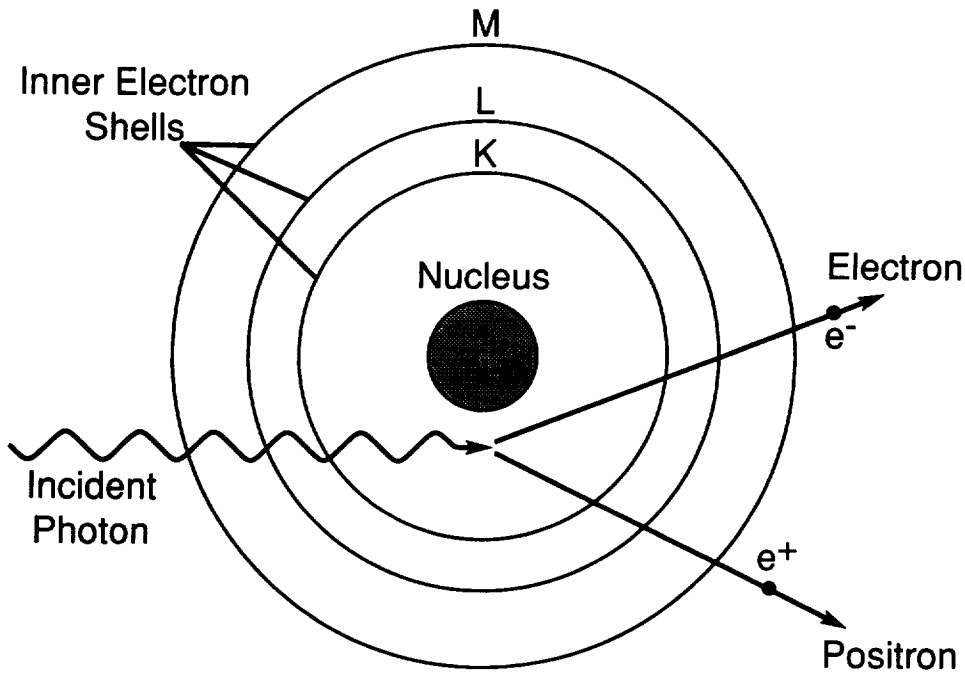

Fig. 3. Pair production. The incident photon is converted into an electron-positron pair in the Coulomb field of an atomic nucleus.

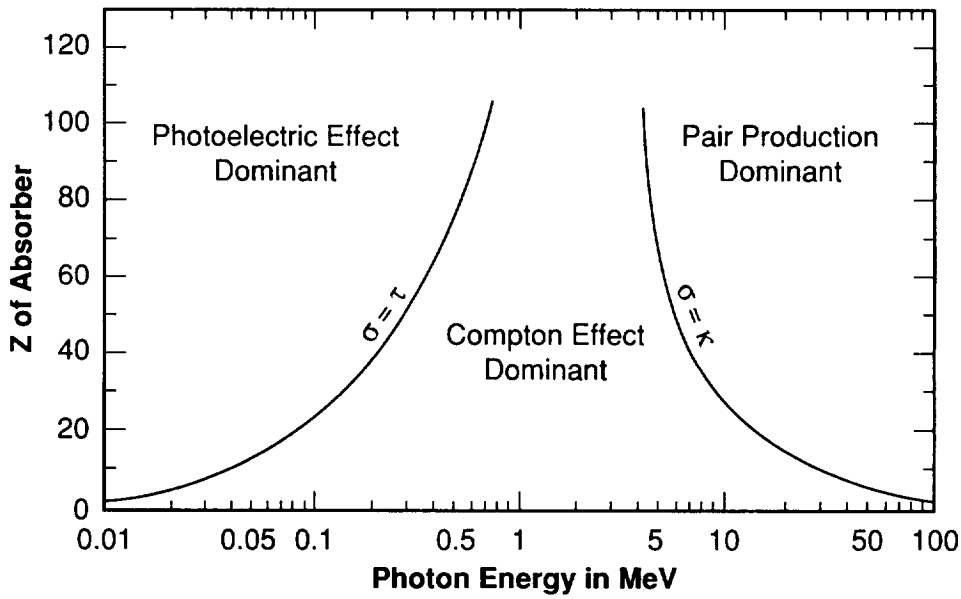

Fig. 4. Cross sections for photon interactions. The Z-dependent boundary regions are shown where the Compton and photoelectric cross sections are equal ($\sigma = \tau$) and where the pair production and Compton cross sections are equal ($\sigma = \kappa$) vs. the initial photon energy (from R. D. Evans, *The Atomic Nucleus*, Copyright 1955, McGraw Hill Book Company, used by permission).

X-Ray and Gamma Ray Astronomy Detectors

II. DETECTOR PRINCIPLES

An x-ray or gamma ray photon interacting with the detector medium liberates charges, and these provide the means to measure the event. In some detectors, the charged particles are collected directly to generate an electrical signal at the output of the detector. In a scintillation detector the charged particles produced by the incident photon generate, through secondary interactions, a light pulse which is converted by a photo detector into an electrical signal. In a calorimeter detector the absorbed energy of the incident photon causes a small temperature increase of the absorber material, and this temperature change is converted into an electrical signal by a suitable thermometer. Regardless of the detector type, each photon interaction generates a discrete electrical signal which is amplified and processed by the detector electronics to obtain information about the properties of the incident radiation (intensity, energy, etc.).

To characterize radiation from celestial x-ray and gamma ray sources, several types of measurements have to be made including flux (intensity), energy, and temporal variations of the received radiation. In addition the angular direction to the source (location of the source on the sky) has to be determined. Detector design is usually optimized to perform one or several of these measurements with high accuracy. Each type of detector has its optimum performance over a limited region of the vast energy spectrum of x-rays and gamma rays.

The flux of the incoming radiation is the number of photons counted by the detector per second and per active detector area. Many cosmic x-ray and gamma ray sources emit very high intensity radiation. However, because of their tremendous distance from Earth the flux seen by the detector is very low. For example the flux from the crab nebula (one of the brighter x-ray sources) is less than 10 photons/cm^2/sec in the energy range from 1-10 keV. A large collecting area is needed to gather enough photons in a reasonable period of time to make reliable (statistically significant) measurements. X-ray and gamma ray detectors are extremely sensitive instruments responding to single photons.

A. ENERGY RESOLUTION

The amplitude of the electrical signal at the detector output is usually a measure of the incident x-ray or gamma ray photon energy. To determine the energy distribution (energy spectrum)

of the received radiation, the pulse signals are sorted in bins according to their amplitude by an electronic pulse height analyzer. Each bin represents a small energy interval (determined by the amplitude discrimination process). The measured energy spectrum of the source can be constructed from the number of pulses collected per bin.

The energy resolution of a detector is defined as its response to a monoenergetic (single spectral line) radiation input. Typically the shape of the detector response is similar to that of a Gaussian distribution centered on the line energy input (Figure 5). The energy resolution is defined as the full width ΔE at half maximum peak height (FWHM) divided by the input energy E_0 and is usually expressed in percent for a given energy. It determines the detector's ability to resolve details in the energy spectrum of the source, for example to separate adjacent spectral lines. Spectroscopy detectors are optimized for high energy resolution, and some can achieve a resolution of better than 1%.

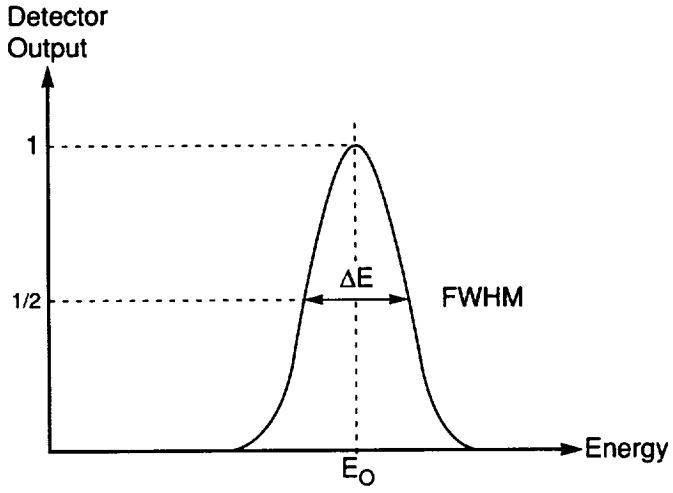

Fig. 5. Energy resolution. The energy resolution of a detector is defined as the full-width-at-half-maximum height (FWHM) of the detector response to monoenergetic radiation.

Detector Principles

The energy resolution of a detector depends on various parameters including the type and design of the detector, the interaction process and sources of random noise in the detector, and the signal electronics. Accurate measurement of the incident photon energy requires that the photon deposit all its energy in the detector absorber; i.e., the primary photon and the secondary interaction products (electrons, photons, etc.) must be stopped completely in the absorber. Even in a large high Z detector there are always events in which only a portion of the primary photon energy is deposited in the absorber and these contribute to the uncertainty in the energy measurement. (For example, in Compton interactions and interactions near the surface or edge of a detector the primary photon or some secondary electrons may escape from the absorber.) Another source of uncertainty in the energy measurement, which applies to all types of detectors and which is always present, is the statistical noise connected with the discrete number of information carriers generated in the interaction event. For example, in a gas-filled counter the photon energy is converted into a discrete number of electron-ion pairs, and in a scintillation counter the primary photon energy is converted into a discrete number of electrons which are emitted from the photocathode of the photomultiplier tube. If the creation of information carriers were a series of completely independent events, Poisson statistics would apply and the standard deviation would be just the square root of the total number of electrons (charge carriers) produced. In this case the FWHM energy resolution would be 2.35 times the standard deviation. Because the creation of information carriers is not a series of completely independent events the statistics of this process is usually found to produce better resolution than would be predicted from Poisson statistics. The Fano factor was introduced to quantify this deviation from Poisson statistics. The energy resolution is now given by

$$\Delta E/E(\%\text{FWHM}) = 2.35 \times \sqrt{F/N} \times 100, \qquad (1)$$

where N is the number of primary electrons produced and F is the Fano factor (F is significantly smaller than 1 for gas-filled and solid state detectors).

B. TIME RESPONSE

A detector counts individual photon interactions in the absorber which occur at random times. The interaction time, the time during which the photon gives off its energy, is very short (nanoseconds in a gas and picoseconds in solid absorbers). It takes a certain time to collect the charges created by the photon interaction in the detector, to produce an electrical signal at the detector output, and to process the signal. During this time interval (dead time) the detector cannot respond to another photon event. To minimize the loss of photon events, the response time of the detector system must be made as short as possible. The response time of a detector is the minimum time separation between two photon events which are still counted as separate interactions. Also, the radiation flux from some x-ray and gamma ray sources shows rather rapid changes (in the millisecond range) which must be detected and recorded accurately by the detector system.

C. IMAGING

One important objective in x-ray and gamma ray astronomy is to determine if a radiation source is associated with a known object visible at a different wavelength (e.g., optical or radio). A detector with a high angular resolution is needed to pinpoint the location of sources on the sky and to resolve details in the image of an extended source. There are several techniques to improve the angular resolution. These include: (1) use of a collimator to restrict the detector's field of view and (2) use of an imaging device in combination with a position-sensitive detector. A position-sensitive detector can determine the location in the detector absorber at which an interaction took place.[6]

D. MECHANICAL COLLIMATOR

A mechanical collimator can be used at the entrance window of a detector to restrict the field of view as indicated in Figure 6. The field of view (2α) depends on the length (L) and the diameter (D) of the apertures of the collimator ($\tan \alpha = D/L$). All photons arriving at angles larger than α are absorbed in the walls of the collimator structure. The angular response of the detector plus collimator has a triangular shape. With practical designs the field of view can be restricted to a few degrees. If the detector is

mounted on a rotating platform (a spinning rocket or satellite) the angular position of a source in the scan direction can be determined from the detector response and platform pointing information with an accuracy dependent upon the detector's field of view. Narrowing the field of view to improve the angular resolution of a scanning detector reduces the observing time of a source per scan and thereby the sensitivity.

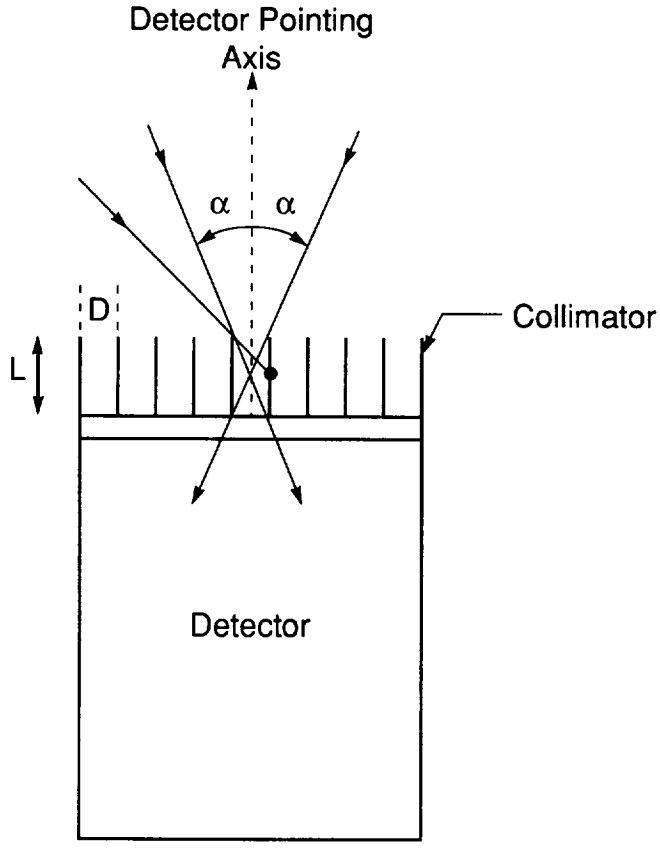

Fig. 6. A typical mechanical collimator. The field of view (2α) is determined by the length and size of the apertures of the collimator. Photons entering from outside the field of view are absorbed in the walls of the collimator.

A further improvement in position determination can be achieved with a rotation modulation collimator. Two planes of wires in front of a detector are rotated about an axis perpendicular to the plane of the wire grids. The rotating grids cause a modulation of the flux from a source. A point source located on the spin axis will not be modulated while the flux from an off-axis source will be modulated with a frequency dependent on the angular distance from the axis. The time phase of the modulation provides the remaining angular coordinate.

Much improved angular resolution can be achieved by using the lunar occultation technique. As the limb of the moon occults a source the corresponding decrease in the flux can be used to determine the source position in the sky with accuracies in the arc sec range. This method, however, is limited with respect to frequency of occurrence and locations on the sky.

E. GRAZING INCIDENCE TELESCOPES

X-rays can be reflected from surfaces at very small (grazing) angles with an efficiency that decreases with photon energy and increases with the reflector's atomic number. For high Z material and soft x-ray energies (below 10 keV) this phenomenon can be used to build focussing x-ray telescopes. Grazing incidence angles are typically less than 1° and at these small angles the effective (projected) reflecting surface area is very small and, as the effective surface area decreases with increasing photon energy, it sets a practical upper energy limit for grazing incidence telescopes. High angular resolution at the arc sec level and better has been achieved with grazing incidence x-ray optics used in conjunction with a position-sensitive detector in the focal plane. In a typical x-ray telescope (e.g., a Wolter Type I telescope) reflections from two surfaces are used to form an x-ray image. The incoming photons are first reflected by a parabolic mirror and then by a hyperbolic mirror before they reach the focal plane (Figure 7). These mirrors are relatively thin cylindrical shells with the inner surface having the shape of a paraboloid or hyperboloid. To increase the effective collecting area, several pairs of parabolic and hyperbolic mirrors are typically nested (located within each other).

X-ray telescopes have been flown on several satellites and new telescopes for future space observatories are under development. The Einstein Observatory satellite (HEAO-B) launched in 1978 carried an x-ray telescope with four nested mirror pairs

which had an effective area of 400 cm^2 at 2.5 keV (30 cm^2 at 4 keV). The telescope had a focal length of 3.4 m, a field of view of 1° and an angular resolution of 4 arc sec. The mirrors were made from fused silica coated with a nickel-chrome alloy. Grazing incidence telescopes will be carried on the Advanced X-Ray Astrophysics Facility (AXAF-I) scheduled for launch in 1998. AXAF-I will have four nested mirror pairs with a maximum effective area of 1000 cm^2 and an angular resolution of 0.5 arc sec. The mirrors will be made of Zerodur coated with iridium.

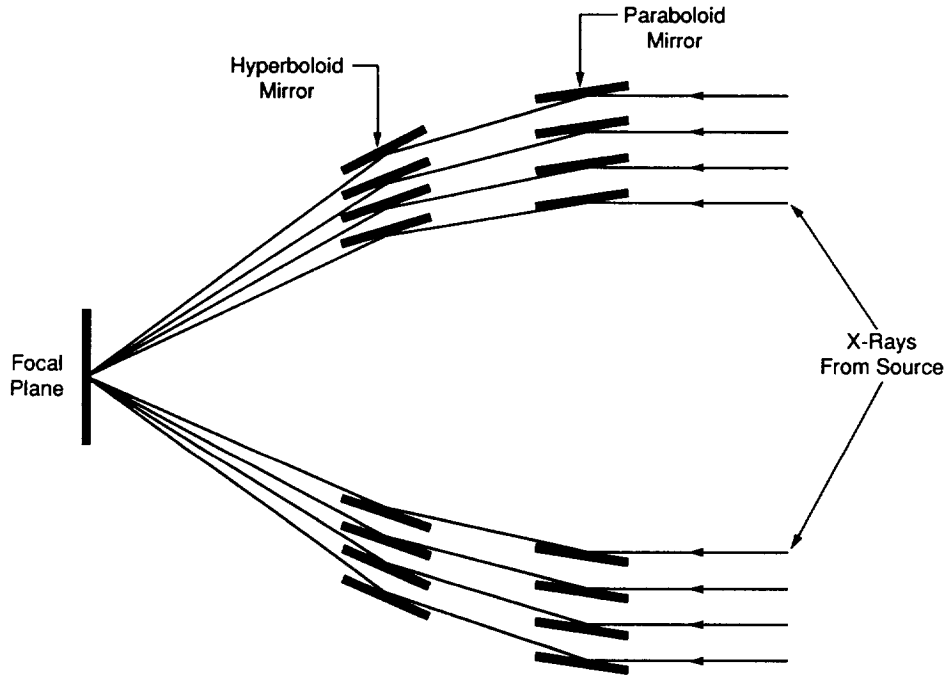

Fig. 7. X-ray telescope optics. Shown are four nested pairs of x-ray mirrors forming a Wolter Type I system. X-rays from a source are first reflected by the paraboloid mirrors and than by the hyperboloid mirrors before they converge in the focal plane of the telescope.

F. CODED-APERTURE MASK

At energies above the range of grazing incidence telescopes coded aperture masks have been used in front of position-sensitive detectors for imaging hard x-ray sources.[8] The mask consists of a pattern containing opaque and transparent areas. Radiation passing through the mask is spatially modulated (coded) by the mask pattern function and casts a shadow of the mask pattern on the position-sensitive detector. Radiation from different points of an extended source arrives at slightly different angles at the detector, each producing a shifted shadow pattern on the detector. The image of the source can be reconstructed from the composite shadow image recorded by the detector using mathematical processing (decoding). The opaque and transparent mask areas are arranged in special patterns, derived mathematically, to ensure optimum image reconstruction. The angular resolution of such a system is dependent upon the element size in the mask pattern, the mask-to-detector distance, and the spatial resolution of the position-sensitive detector. Angular resolutions of a few arc minutes are typical. Figure 8 gives an example of a coded-aperture system.

G. COMPTON TELESCOPES

For gamma rays above a few MeV the Compton scattering process can be used to determine the direction of motion of the incident photon.[2] With increasing photon energy the angular distribution of the Compton scattered photon and electron becomes narrower, and by measuring their direction of motion one can determine the direction of motion of the incident photon (Compton telescope). At higher gamma ray energies where pair production dominates, the direction of motion of the created secondary electron-positron pair can be measured to reconstruct the direction of the primary photon[2] (see section III.D).

H. BACKGROUND

The weak photon flux from celestial x-ray and gamma ray sources has to compete with the ever-present radiation background at the detector.[1-3] Several components contribute to the background in space-borne detectors. There is a diffuse, isotropic x-ray and gamma ray background across most of the spectrum. A

second component is cosmic rays (mostly protons) which interact with the detector and are counted as photons. The flux of cosmic ray particles is larger than the photon flux from most celestial x-ray and gamma ray sources. In addition their interaction with the structures of the detector and the spacecraft generates secondary particles and photons which can interact with the detector. The Earth's radiation belts (trapped electrons and protons) are a serious problem for space-borne detectors depending on satellite altitude and orbit inclination. Cosmic rays interact with the Earth's atmosphere, and the resulting radiation is scattered back to the orbiting spacecraft. Additional background radiation is caused by natural and induced radioactivity in spacecraft and detector materials. Induced radioactivity results from the interaction of cosmic rays and radiation belt protons.

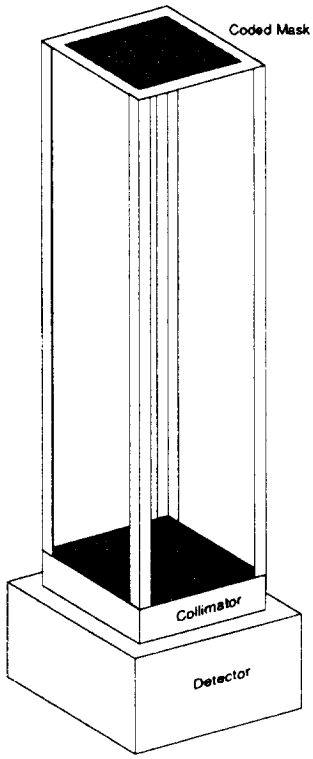

Fig. 8. A typical coded-aperture imaging system.

X-Ray and Gamma Ray Astronomy Detectors

The ratio of source photons to background photons (signal-to-noise ratio, S/N) is a major factor in determining the minimum detectable flux from a source. Typically, for non-focussing systems, observations in x-ray and gamma astronomy are background limited, where the size of the background flux determines the minimum detectable source flux. For focussing systems, where the source flux is concentrated into a small detector area, a very large increase in the S/N ratio is possible and many observations are photon limited, i.e., limited by the small number of source photons registered.

I. SHIELDING

Different shielding techniques have been developed to reduce background radiation. Radiation which enters the detector from the sides and from the rear can be eliminated or reduced by enclosing the detector (except for the window) in a metal shield which absorbs the unwanted radiation (passive shielding). Passive shielding against high-energy radiation requires heavy shields which are undesirable for space-borne detectors. A more efficient technique is active shielding which uses one or several additional detectors surrounding the primary detector (see section IV). With proper geometrical arrangement of the secondary or shield detector, radiation from outside the field of view would have to penetrate both the shield and the primary detector causing simultaneous output from both detectors. An electronic anticoincidence circuit rejects events yielding simultaneous detector responses (anticoincidence shield). Charged particles (e.g., cosmic rays) entering through the detector window can be discriminated against by using a secondary detector with a low cross section for photons in front of the primary detector. Charged particles interact with both detectors causing simultaneous output signals which are then rejected; whereas, photons, which interact only with the higher cross section primary detector, are counted. In addition to shielding, background radiation contained in the recorded detector data can to some extent be accounted for by detector calibration in the laboratory and from calculations of the background radiation environment.

III. GAS-FILLED DETECTORS

A. INTRODUCTION

Gas-filled detectors function by detecting the charge liberated when a photon interacts with the fill medium. In the energy range where these detectors are normally employed this interaction is predominantly the photoelectric effect (see section I) and the charge is liberated through ionizing collisions as the initial photoelectron, and de-excitation products, come to rest in the detector gas. The number of free electrons produced is proportional to the absorbed photon's energy and is dependent on the characteristics of the fill gas. Typically, a mean energy of 20-25 eV is needed to produce an electron-ion pair so that a 20-keV incident photon would produce around 1000 electrons. As the Fano factor for commonly-used detector gases is in the range 0.2-0.3, the Fano limiting resolution for gas-filled detectors would be 3%-4% FWHM at 20 keV, were there no other contributing factors (see section II.A for an explanation of the statistics of primary information carriers).

There are many different types of gas-filled detectors. Ionization chambers simply register the initial ionization produced but are not really useful for x-ray and gamma rays because at the energies where gas-filled detectors are efficient, typically below 100 keV, the signals are too small to drive processing electronics. Proportional counters and gas scintillation proportional counters internally amplify the signal to useful levels, even for very low-energy photons and, hence, have found widespread use in astronomy. Geiger counters produce very large saturated pulses when irradiated but have no energy information and as a consequence are not used directly in this application, but a derivative of this device, the spark chamber, is sometimes used for high-energy photon detection. Each of these instruments, as used or planned for use in x-ray and gamma ray astronomy, will now be described in turn.

B. PROPORTIONAL COUNTERS

Proportional counters rely on the phenomenon of gas multiplication to amplify the signal from the tiny primary electron cloud, typically containing 10^3 electrons for a 20-keV absorbed photon, to the 10^5-10^7 electrons necessary for driving

preamplifiers and processing electronics. The device came of age in the late 1940s, early 1950s[9] and has since developed into a highly sophisticated instrument for use in such areas as high-energy physics from which the bulk of the later development work has come.[10]

In its simplest form, as shown in Figure 9, the proportional counter consists of a single fine wire, the anode, concentric with a gas-filled cylinder which forms the cathode. A positive high potential (V), relative to the cathode, is applied to the anode, and electrons liberated in the gas by absorbed photons drift toward the central wire. The field E at a distance r from the anode is given by

$$E(r) = V[r \ln(b/a)], \tag{2}$$

where b is the cathode inner radius and a is the anode radius. The field therefore increases as the wire is approached. At a distance of a few wire radii from the wire surface the drifting primary electrons gain enough kinetic energy from the electric field to ionize the fill gas and produce secondary electrons which, in turn, have further ionizing collisions. In this way an avalanche is produced close to the anode wire surface in which each primary electron produces a large, but roughly constant, number of secondaries. Gas multiplication factors, usually termed gas gain, of $>10^4$ are typically possible before saturation sets in, at which point the charge in the leading edge of the avalanche becomes so great that the local electric field is distorted and non-linearities in response occur. The gain is dependent on the applied voltage, the detector geometry, and the fill gas. Typical proportional counters would have a 25 μm diameter anode, an anode-cathode distance of 1-2 cm, and would be filled to a pressure of 1 atmosphere. A thin entrance window would permit x-rays to enter the chamber. They are not restricted solely to this coaxial configuration and are sometimes used with other geometries such as the parallel field case where charge multiplication takes place between pairs of mesh grids.[11] The term proportional counter is used in all cases as the output signal size remains proportional to the input photon energy. The fact that the avalanche region is very close to the wire for the coaxial geometry ensures that each electron cloud experiences the same multiplication factor regardless of where the original photon is absorbed in the detector.

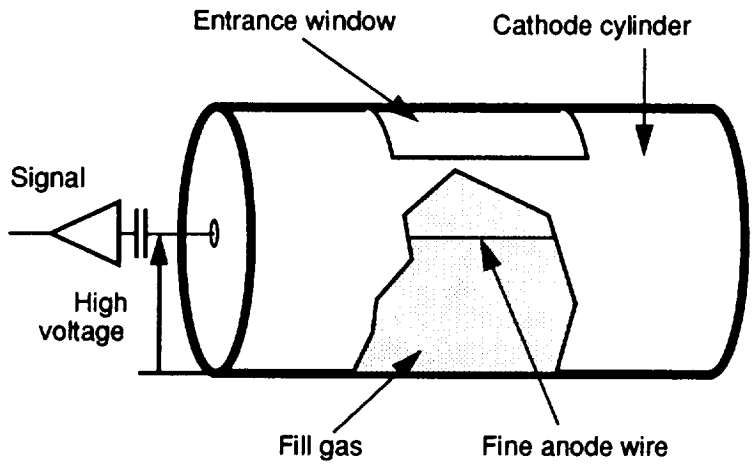

Fig. 9. Schematic of a single-wire proportional counter.

The signals from a proportional counter typically have very fast initial rise times, less than 1 μs, due to the high velocity of the charges in the intense field near the wire. The bulk of the signal is in fact induced by the motion of the positive ions away from the anode as these move through a much greater potential difference than the electrons. These ions move very rapidly at first but then slow down as regions of weaker field are reached away from the anode. The total collection time for the ions can be ≈100 μs but the signal is normally shaped with a short electronic time constant so that only the initial fast rise time is seen by the processing electronics.

The choice of fill gas is determined by the application. Noble gases are usually chosen over complex polyatomic molecules as the latter have many rotational and vibrational energy levels which can waste energy that could otherwise have gone into ionization. Under most circumstances, however, pure noble gases alone do not operate stably at moderate to high gas gains due to the emission of ultraviolet photons in the avalanche. These photons can cause ionization in the walls of the detector and the resulting free electrons can drift to the wire and produce serious after pulses. To prevent this, a small quantity, usually a few percent, of a polyatomic quench gas is added to provide stable operation either by direct absorption of the photons or through de-excitation of the noble gas atoms before ultraviolet emission occurs. Typical fill gases in x-ray and gamma ray astronomy are argon and xenon with carbon dioxide or methane as quench ad-

ditives. Xenon ($Z = 54$) is preferable to argon ($Z = 18$) at energies above 10-20 keV as the photoelectric cross section scales as Z^n, where n is between 4 and 5. Even so, xenon quickly becomes transparent at higher energies so that with few exceptions, proportional counters are rarely used above 100 keV.

The choice of quench gas can also effect the performance of the counter. Pure noble gases have low electron drift velocities and are very susceptible to electronegative contaminants which can remove electrons from the drifting primary charge cloud. The addition of a small percentage of methane can speed up the drift by more than a factor of 10 and render the counter relatively insensitive to contaminants which outgas from the detector walls and interior components. For long lifetime applications another consideration is the buildup of deposits on the anode wire through the gradual polymerization of the quench gas. This detector aging is most noticeable in methane-quenched detectors yet appears not to occur when carbon dioxide is used; consequently, this latter quench gas has been widely used in satellite applications.[12]

More exotic quench gases can be utilized to improve the performance of the standard proportional counter. The so-called Penning gas mixtures are ones in which the quench gas is specifically chosen to collisionally de-excite long-lived states in the noble gas resulting in subsequent ionization of the quench additive. This increase in ionization improves the energy resolution of the detector and reduces the high voltage requirements.[13]

The energy resolution of a proportional counter consists of two components. The first is governed by the statistics of the initial photoionization process and the second comes about from the charge multiplication process. The standard formula for this resolution at energy E is

$$\Delta E(\text{FWHM}) = 2.35[\{W(F+A)\}/E]^{0.5}, \tag{3}$$

where W is the mean energy to form an electron-ion pair, F is the Fano factor (see section II), and A is the relative variance of the multiplication factor for a single electron. The multiplication variation comes about from small changes in the relative amounts of energy going into excitation versus ionization in the first few steps of the avalanche and results in corresponding changes in the amplification factor from event to event. This component is by far the larger of the two $(F + A)$ and dominates the energy resolution of practical proportional counters. Typical

values are around 0.2 for F, 0.6 for A, and W = 26 eV for argon + methane, resulting in an energy resolution of around 14% at 5.9 keV for a single wire detector. Despite much work with special gas mixtures and different geometries, it has proven very difficult to improve on this value.

- Multiwire Proportional Counters

To satisfy the desire for large collecting areas and position sensitivity, the Multiwire Proportional Counter (MWPC) was developed.[10] This device, shown schematically in Figure 10, consists of planes of anode wires sandwiched between planes of cathode wires to form a series of cells, each of which can be looked on as a single wall-less proportional counter. The full sensitive volume of the detector can either be filled with these cells, Figure 10a, as was the case with the monitor proportional counters on the Einstein satellite,[14] the proposed proportional counter array for the X-Ray Timing Explorer (XTE),[15] and the large area counters on the GINGA satellite (Table 1), or there can be an absorption and drift region followed by a sense region, as shown in Figure 10b. The latter configuration is typically used if position sensing is required, as is the case when the detector is at the focus of an x-ray reflecting telescope or in a coded aperture system (see section II).

Table 1. Characteristics of the GINGA Large-Area Counter (LAC)[16]

Sensitive Area	4000 cm^2 (eight detectors)
Window	62 μm beryllium
Fill Gas	75% argon + 20% xenon + 5% carbon dioxide @ 1.86 atm
Energy Range	1.5-37 keV
Energy Resolution	18% FWHM at 5.9 keV
Time Resolution	980 μsec

The front end of the MWPC often has a collimator designed both to define a region of the sky from which to accept x-rays and to support the thin entrance window which permits x- and gamma rays to enter the detector. Sometimes the collimator is omitted, as at the focus of telescopes, and a mesh provides window support. For low-energy applications, below a few keV, these windows are normally made from thin plastics (down to 1 μm) coated with carbon or aluminum to make them conducting and prevent charge from building up on their inner surface. At

higher energies, beryllium or even aluminum foils or sheets can be used and these can be quite "thick." For balloon-borne detectors, where the residual atmosphere cuts off the low-energy flux below 20 keV, aluminum windows as thick as several hundred micron can be utilized without loss of signal.

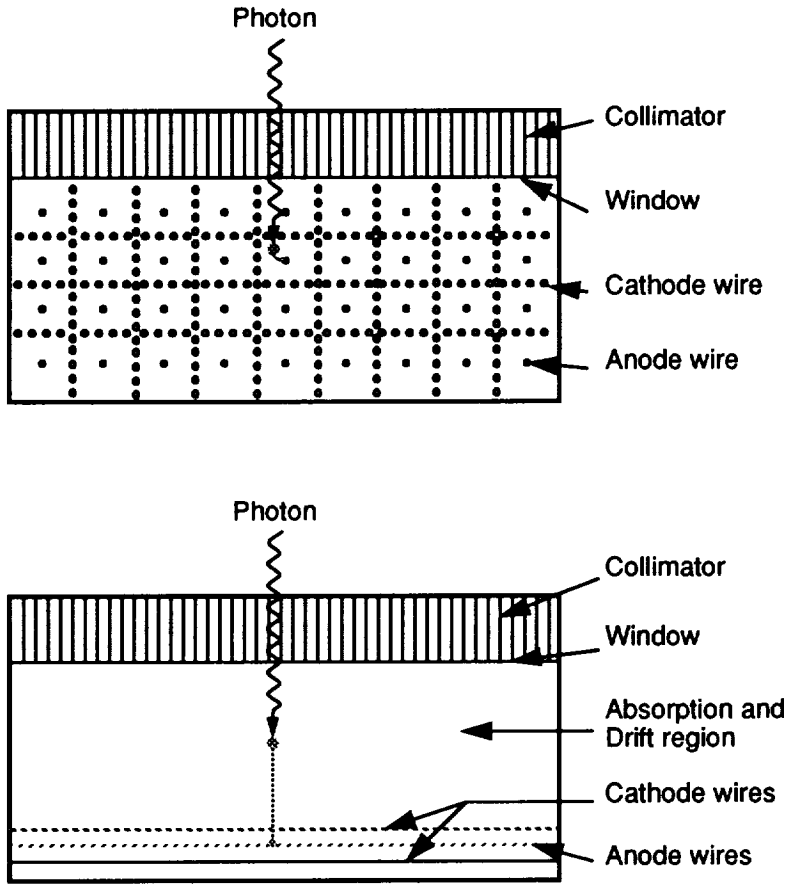

Fig. 10. Different approaches to Multiwire Proportional Counter (MWPC) design.

Many applications, for example in x-ray telescopes, demand that the MWPC be position sensitive and there exist a multitude of schemes for deriving the position of events within the counter. These usually rely on induced signals in mutually orthogonal top and bottom cathode planes. By connecting the cathode wires, either individually or in small groups, to separate preamplifiers and noting which channels trigger and the amplitude of their signals, the original interaction site can be recovered with high precision. This is the so-called center of gravity technique[17] as depicted in Figure 11a and utilized on the position-sensitive proportional counter (PSPC) at the focus of the grazing incident telescope of the ROSAT satellite.[18] Details of this instrument are given in Table 2. Other schemes which are employed include coupling the cathodes to delay lines and measuring the difference in arrival time at the two ends of each line, as shown in Figure 11b, or connecting successive cathode wire groups through resistors and measuring how this distributed resistance, coupled with the capacitance of each wire subgroup, modifies the rise time of the signal as a function of position in the detector (Figure 11c).

Table 2. Specification for the ROSAT PSPC[18]

Sensitive Area	8 cm diameter
Drift and Absorption Region	8 μm
Window	1 μm polypropylene with 50 μg/cm^2 carbon
Fill Gas	65% argon + 20% xenon + 15% methane @ 1.5 atm
Energy Range	0.1-2.0 keV
Energy Resolution	43% FWHM at 0.93 keV
Spatial Resolution	250 μm at 0.93 keV
Time Resolution	120 μsec

The ultimate spatial resolution limit is set by diffusion in the detection gas and the finite range of the initial photoelectron and de-excitation products. The former is the dominant factor at low energies where the lateral spread of the charge cloud due to thermal motion of the electrons and the small number of electrons within the cloud makes the determination of the exact centroid imprecise. Typical diffusion limits, which scale as the square root of drift distance divided by pressure, are around 1/10 mm FWHM at 6 keV for a few cm drift in 1 atmosphere of gas. At higher energies the ejected photoelectron has a non-negligible range and this quickly dominates the spatial resolution. At 30 keV

the spatial resolution is several mm in 2 atmospheres of argon and at 60 keV it is more than 1 cm.[19] If high spatial resolution is required at high energies then heavier gases must be used at elevated pressures to reduce the electron track length. In 10 atmospheres of xenon, the spatial resolution at 100 keV would be sub-millimeter.

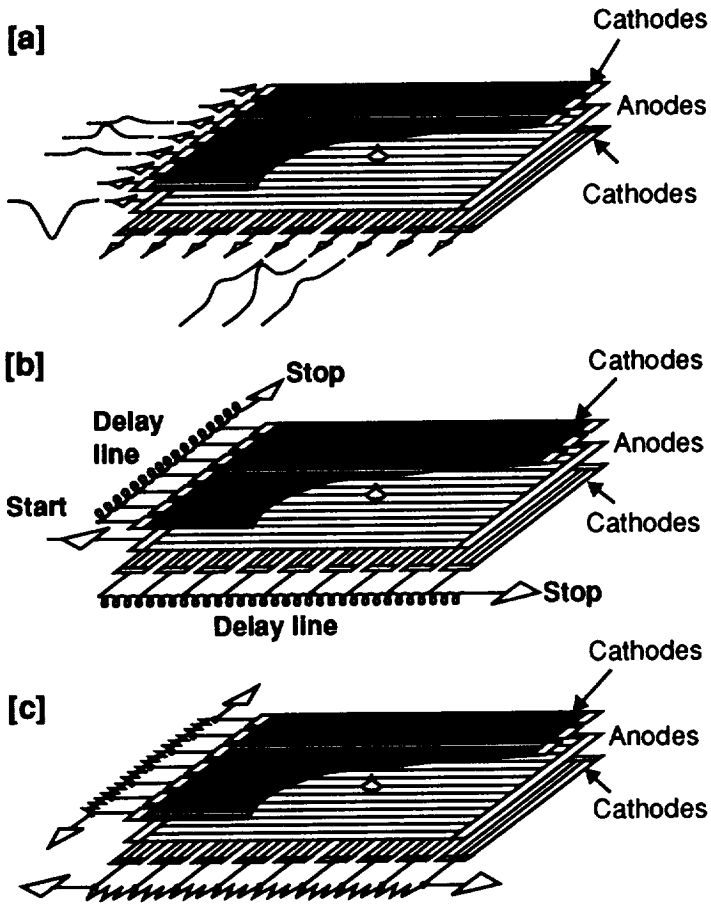

Fig. 11. Various schemes used for position readout of cathode signals.

While the modern MWPC is highly developed and bears little resemblance to the original single wire proportional counter, further improvements are still being sought. The desire to improve the timing properties of the MWPC for particle research led to the development of the microstrip proportional counter

which has many features desirable for astronomy. In these devices, the usual discrete anode and cathode wires are replaced by conducting strips on a partially insulating substrate (Figure 12). Fabricated using integrated circuit-type photolithographic processes, they offer very high spatial accuracies and uniformity together with the capability of producing extremely fine electrode structures down to the 1 micron level, far beyond the 12.5 micron mechanical limit for wires in practical counters. As the energy resolution of MWPCs is often dominated by geometrical inaccuracies in wire placement, which affect the electric field from wire to wire, as well as anode uniformity and diameter, microstrip proportional counters offer the promise of superior energy performance; <11% FWHM at 6 keV has already been reported, along with reduced operating voltages, faster signal rise times (due to the very intense fields around the ultra-fine anodes), and the reduced likelihood of wire breakage.[20]

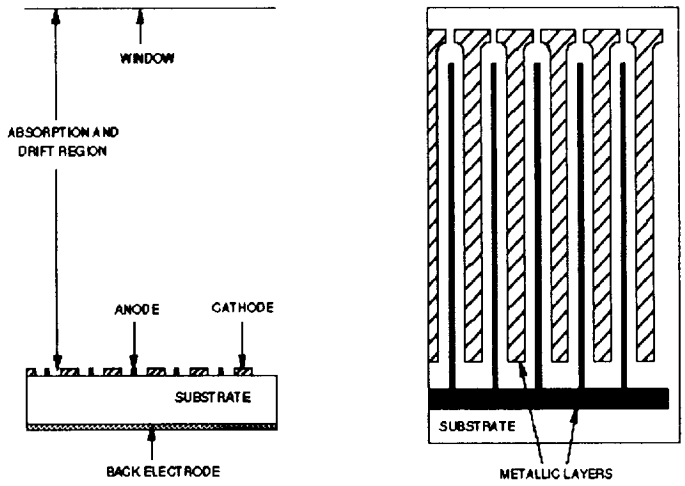

Fig. 12. Schematic of a microstrip proportional counter.

C GAS SCINTILLATION PROPORTIONAL COUNTERS

The gas scintillation proportional counter (GSPC) is a variant of the standard proportional counter in which the electric field is kept just below that necessary for charge multiplication.[21] Under these conditions the primary electrons drift into a high field region and each gains enough energy to excite the fill gas atoms but not to ionize them. This results in a burst of charac-

teristic ultraviolet photons whose intensity is proportional to the energy of the initial x- or gamma ray. This scintillation light, which is around 150-200 nm for pure xenon, typically contains tens of thousands of photons and is registered by quartz window photomultiplier tubes as is the case with solid scintillators (see section IV). Figure 13 gives a schematic representation of a typical GSPC.

The attraction of the GSPC derives from the fact that the emission of scintillation photons is a series of completely independent events and therefore the energy resolution is dependent on the statistics of the final number of photons collected. This is in contrast to the standard proportional counter where the statistics is set not by the final number of electrons but by fluctuations at the beginning of the avalanche process. In the limit, for large light yield and good collection efficiency, the energy resolution of the GSPC can approach the Fano limit described in section III.A and thus can be a factor of 2 better than the standard proportional counter.

The geometry of the GSPC, as shown in Figure 13, is very similar to that of the MWPC with a low field absorption and drift region and a high field scintillation region which is normally defined by a parallel pair of grids and spans several mm to enhance the light yield. Sometimes these two regions are combined into a so-called "driftless" GSPC having a high field throughout the whole detector volume.[22] In this configuration the amount of light produced for a given input energy is variable and depends on the penetration depth of the initial x- or gamma ray. The original energy is then recovered by measuring not only the light yield but the duration of the light signal or burst length. The advantage of the driftless GSPC is that the interior electric field is very high throughout and this ensures rapid registration of each event before any losses of charge to the entrance window or to electronegative contaminants in the detector gas. It also removes the need for drifting through grids delineating the drift and scintillation region which can also result in charge loss.

The original GSPC was developed in 1972 and since then several instruments have been flown on sounding rockets and satellites. The GSPC onboard the EXOSAT satellite was a non-imaging device with an effective area of 100 cm^2 which operated over the energy range 2-40 keV. Its energy resolution was 10% at 6 keV.[23] Imaging GSPCs are actively being developed and there are a number of schemes for position sensing. A common arrangement is to use some form of imaging photomultiplier tube to determine the centroid of the light distribution. Such a technique is used on the driftless imaging GSPC being developed for the fo-

cal plane of an x-ray telescope on the Italian SAX mission[24] and for the conventional GSPC used as a focal plane instrument on the Japanese ASTRO-D (ASCA) mission.[25] Details of these two instruments are given in Table 3.

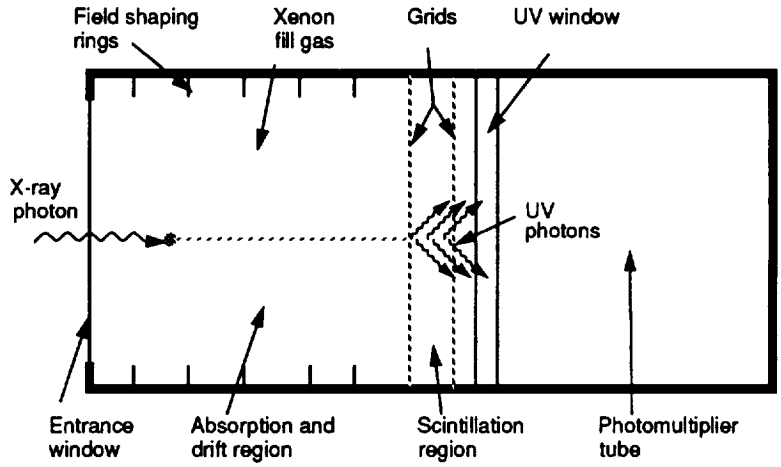

Fig. 13. A conventional Gas Scintillation Proportional Counter (GSPC) with drift volume.

Table 3. Characteristics of the GSPCs for the ASTRO-D[25] and SAX[24] Missions

	ASTRO-D	SAX (LEGSPC)
Effective Area	50 mm dia.	30 mm dia.
Effective Range	0.7-20 keV	0.1-10 keV
Energy Resolution (5.9 keV)	<8% FWHM	7.0%
Position Resolution (5.9 keV)	0.5 mm	0.9 mm
Time Resolution	61 μsec	---

Finally, a group at Berkeley is developing a very high pressure large-area imaging GSPC for use on a high-altitude balloon platform. This device will have a sensitive area of over 1000 cm^2 and will contain a 22 cm depth of xenon gas at 20 atm.[26] To avoid the mechanical problems of large-area ultraviolet transmitting windows it utilizes a novel position-sensing readout scheme consisting of crossed arrays of wave shifting optical fibers which exit the pressure vessel and are read out by an array of phototubes. The instrument is designed to operate from the atmospheric cut-off point, 20-30 keV, up to several hundred keV.

D. GAS-FILLED SPARK CHAMBERS

Spark chambers have been widely used as charged particle track detectors . Here, the passage of the particle ionizes a fill gas in a volume containing electrodes connected to a pulsable high voltage power supply. On the command of a trigger circuit, a voltage is applied of such a magnitude that avalanches and streamers are formed at the initial ionization site. These sparks are registered either photographically, or electronically, and the charges formed in the spark are then swept from the region by a clearing electric field to ready the chamber for the next particle. The trigger is typically supplied by a plastic scintillator through which the charge particle must pass on its way to the spark chamber.

With a suitable conversion medium the spark chamber can be used for high-energy gamma ray detection as is the case with the EGRET (Energetic Gamma Ray Experiment Telescope) on board the Compton Gamma Ray Observatory.[27,28] This instrument uses a stack of 28 spark chamber modules filled with 99.5% neon + 0.25% argon + 0.25% ethane at atmospheric pressure and interleaved with tantalum foils which act as the converter. High-energy photons in the range 20 MeV to 30 GeV interact in the tantalum via pair production (see section I.C) to give an electron positron pair, the downward trajectories of which are registered by the spark chamber modules below the interaction site. Reconstruction of these trajectories enables the initial direction of the source photon to be determined.

Figure 14 gives a schematic of the EGRET instrument. The device is triggered by a central plastic scintillator and, if a suitable signal has been received from a second lower scintillator and no signal received from an outer anticoincidence shield, the high voltage is supplied to the spark chambers. The sparks occur between orthogonal planes of wire grids in which each wire threads a separate magnetic core. The resulting current pulse sets the relevant cores corresponding to the spark locations in each chamber module and these are read out after the event by the processing electronics enabling the full tracks to be reconstructed. The total energy of the event is derived from a thick (20 cm) NaI scintillator positioned below the spark chamber with a correction for the charged particle's energy losses through the tantalum foils. Details of the characteristics of the EGRET instrument are given in Table 4. Similar, though less complex instruments, were flown on the SAS-2 and COS-B gamma ray satellites.

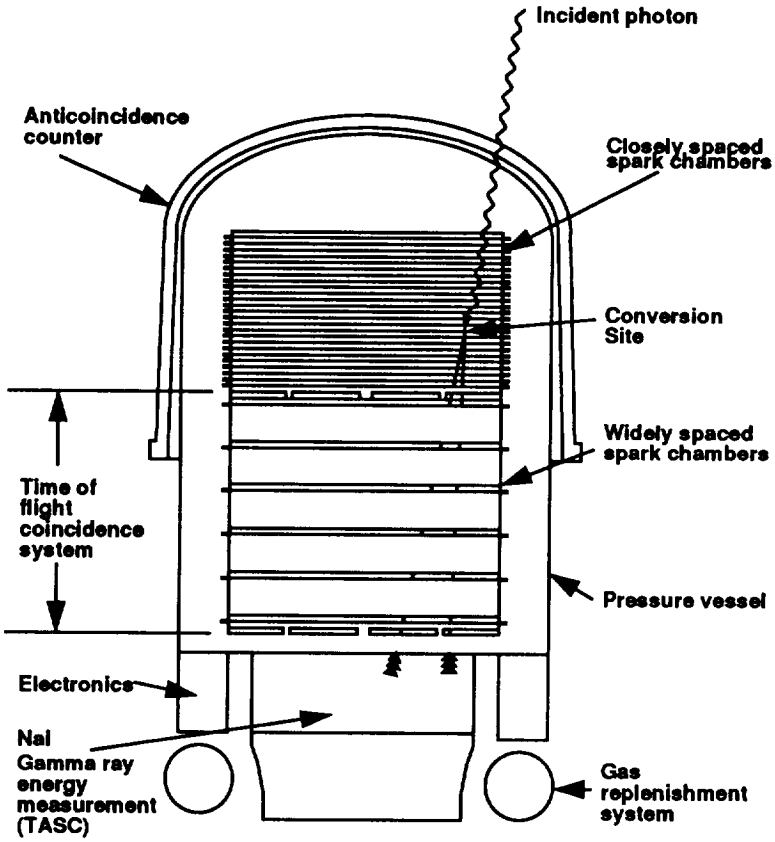

Fig. 14. Schematic arrangement of the Energetic Gamma Ray Experiment Telescope (EGRET) on the Compton Gamma Ray Observatory.

Table 4. Characteristics of the EGRET Instrument[27,28]

Geometric Area	6500 cm^2
Conversion Efficiency	30% at 100 MeV
Energy Range	20 MeV to 30 GeV
Energy Resolution	<25% FWHM from 100 MeV to 10 GeV
Field of View	40° FWHM
Time Resolution	100 μsec
Spatial Resolution for Spark Location	<1 mm
Angular Resolution	10 arc min at high energies degrading to a few degrees at low energies

X-Ray and Gamma Ray Astronomy Detectors

IV. SOLID AND LIQUID SCINTILLATION DETECTORS

Scintillation detectors have found wide applications not only in x-ray and gamma ray astronomy but also in many other areas of radiation detection and measurement.[29] An x-ray or gamma ray photon entering a scintillation detector interacts with the atoms in the scintillator material which results in a flash of light (scintillation). The light pulse is detected by a photo-sensitive detector such as a photomultiplier tube (PMT) or photo diode, which generates an electrical pulse signal for each incident x-ray or gamma ray photon. The intensity of the light pulse is a measure of the energy of the incident photon. The scintillator material can be in the form of a gas, liquid or solid. This section deals with solid and liquid scintillators (gas scintillators are discussed in section III.C). The basic components of a scintillation detector (Figure 17a) are the primary scintillator (S1), the light collector, the PMT, and shields against undesired radiation (S2, S3).

The scintillator material must be transparent to the light generated in the scintillator, it should have a high efficiency in converting gamma ray photon energy into light energy, and the light output should be proportional to the photon energy deposited in the scintillator over a large portion of the photon energy spectrum. Its index of refraction should be close to that of glass (approximately 1.5) to permit efficient optical coupling with the photomultiplier tube or scintillator window. The duration of the light flash (luminescence) should be very short to obtain fast electrical pulses, and the scintillator material should be available in large sizes to achieve large detector collecting areas.

A. INORGANIC SCINTILLATORS

Table 5 shows the properties of a selection of scintillators which are of interest in x-ray and gamma ray astronomy. Among the many available inorganic scintillator materials,[5] alkali halide crystals have the best light output and linearity and have good stopping power for the incident photon because of their relatively high atomic Z number and density. For accurate photon energy measurement the photon and all secondary electrons and photons must be stopped in the scintillator material. The most frequently used scintillators for high-energy astronomy are

sodium iodide crystals activated with thallium NaI(Tl) and cesium iodide activated with thallium CsI(Tl) or with sodium CsI(Na).

Table 5. Properties of a Few Selected Scintillators

Scintillator Material	Density g/cm^3	Atomic Number Z	Relative Scintillation Effic. (%)	Wave-length nm	Decay Const. μs
Inorganic Scintillators					
NaI(Tl)	3.67	11/53/81	100	415	0.23
CsI(Tl)	4.51	55/53/81	45	540	1.00
CsI(Na)	4.51	55/53/11	85	420	0.63
BGO ($Bi_4Ge_3O_{12}$)	7.13	83/32/8	8	505	0.30
Typical Plastic Scintillator					
BC-400	1.03	- -	28	423	0.0024
Typical Liquid Scintillator					
BC-501	0.87	- -	44	425	0.0037

NOTES: The wavelengths are shown for maximum light emission. Scintillation efficiency is shown relative to NaI(Tl), and the atomic numbers are given for the individual scintillator elements. (Data are from references [5] and [29] and BICRON Corp. Catalog.)

Activators are small amounts of impurities which are added to the pure crystal to improve the light output. In the case of NaI crystals a small amount (10^{-3} mol fraction) of thallium is used as an activator. The scintillation light is emitted by the activator atoms. The activator shifts the energy transitions caused by the incident gamma ray photon in the scintillator to the visible wavelength region for detection by a photo detector. Among inorganic scintillators, NaI(Tl) has a very high absolute overall efficiency (11%) for converting photon energy to light and the light output is relatively linear over a large region of the x-ray and gamma ray energy spectrum. NaI(Tl) crystals make excellent photon detectors and spectrometers from approximately 10 keV into the high-energy gamma ray region.

The initial photon interaction with the scintillator is followed by a complicated sequence of secondary interactions which lead to the emission of light. The incident photon generates secondary electron-hole pairs which diffuse to the site of an activator atom and raise the atom to an excited state. When the activator atom de-excites, the energy is emitted as a visible light flash. The decay time of the light pulse determines the time resolution of the de-

tector. The scintillation of a NaI(Tl) crystal has a peak at a wavelength of 4200 Å (420 nm) which matches the peak sensitivity of some common photomultiplier tubes (Figure 15). NaI(Tl) crystals have the advantage that they can be grown to the large sizes needed to obtain sensitive and efficient detectors for astronomical applications. These crystals are hygroscopic and a hermetic enclosure is needed to prevent deterioration caused by atmospheric humidity. The scintillator crystal is usually coupled by a semi-rigid optical cement to a glass or quartz window which is part of the hermetic enclosure. The properties of scintillators (e.g., scintillation efficiency and decay time) are temperature dependent.

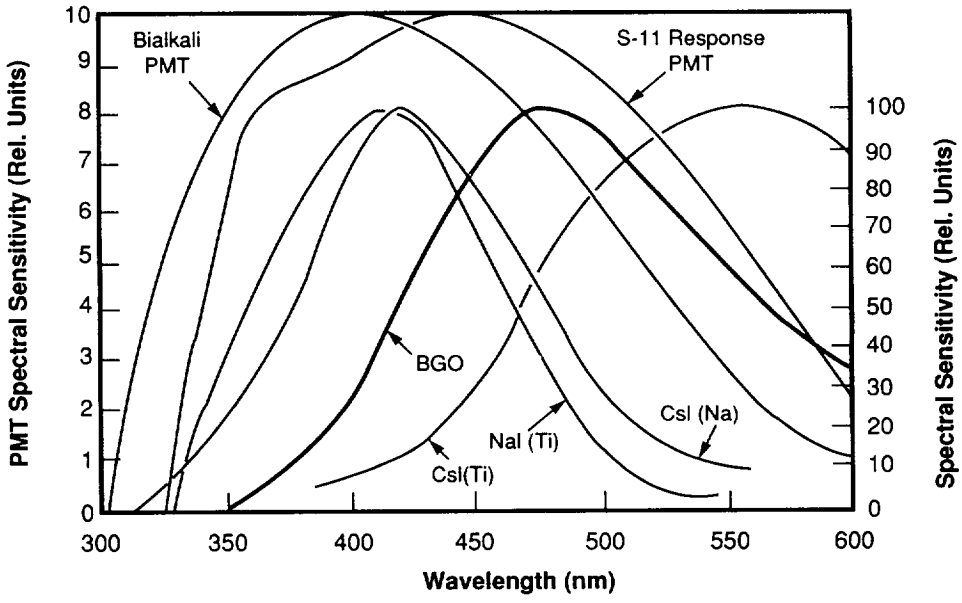

Fig. 15. Scintillator emission spectra for several common inorganic scintillators. Also shown are the response curves for two widely used photocathodes (from G. F. Knoll, *Radiation Detection and Measurement*, Second Ed., 1989, John Wiley & Sons, used by permission).

Another inorganic scintillator material of interest is BGO (bismuth germanate, $Bi_4Ge_3O_{12}$). Its main attraction is its high density (7 g/cm^3) and large atomic number (83 for Bi) which give BGO the largest cross section per unit volume of common scintillator materials for photoelectric gamma ray absorption.

Unfortunately, the light output of BGO is relatively low (approximately 10% of NaI(Tl)). However, BGO has excellent mechanical properties and is not hygroscopic. Because it is presently not available in large sizes, it has not yet found applications in primary detectors for astronomy, but is frequently used as an active shield.

B. ORGANIC SCINTILLATORS

Organic scintillators are available as organic crystals, liquids, and plastic material. Compared with inorganic scintillators, plastic scintillators have lower atomic numbers and lower density with a correspondingly lower absorption for photons. For these reasons, plastic scintillators are not frequently used as primary photon detectors in astronomical applications. However, they have an important application in active shielding of photon detectors to discriminate against charged particle radiation. The decay time of the scintillation pulse in plastic scintillators is usually much shorter (nanoseconds) than in inorganic scintillators. A plastic scintillator consists of an organic scintillator dissolved in polymerized plastic (e.g., polystyrene). Plastic scintillators can be fabricated in various shapes and in large sizes. Organic scintillators are also used in liquid form. Liquid scintillators consist of organic scintillator material dissolved in an appropriate solvent and a variety of liquid scintillators is available commercially.

C. LIGHT COLLECTION

The light generated in a scintillator is emitted in all directions and only a fraction of the light photons travel directly to the photomultiplier. Of the remaining photons as many as possible must be reflected back into the photomultiplier. The energy resolution of a detector is affected by the light collection efficiency and by variations in the collection efficiency across the detector area. Scintillator crystals not larger than the PMT window are coupled directly to the PMT window which provides efficient and uniform light collection. In large-area detectors several PMTs may be coupled to the scintillator surface or a light collector can be used between the scintillator and the PMT to improve collection efficiency. The light collector could be a light guide (e.g., made of Lucite) or a diffusion box. The internal surface of a

diffusion box is coated with a reflective layer (e.g., aluminum oxide or magnesium oxide) which provides efficient diffuse reflection of the scintillation light. In the diffusion box, the light undergoes multiple reflections which results in uniformity of response at the expense of collection efficiency. The entrance surface and edge of the scintillator are covered with a thin metal foil or a diffuse reflection sheet to prevent loss of scintillation light. For detection of low-energy gamma ray photons the reflecting layer must be kept thin to avoid photon absorption. Light may be lost at the interface of the scintillator with the PMT or the light collector. A difference in the refractive indices at the interface can lead to total internal reflection or partial reflection depending on the angle at which the scintillation light strikes the interface and on the ratio of the two refractive indices. Ideally the two indices of refraction should be identical for maximum light transmission, but this is rarely achieved.

D. PHOTOMULTIPLIER

A photomultiplier tube (PMT) combines the functions of photon detection and electron multiplication in one unit.[5] The basic elements of a PMT which are housed in a vacuum enclosure are illustrated in Figure 16. The inside surface of the entrance window is coated with a thin photo-sensitive layer, the photocathode. Light entering through the window interacts with the photocathode (photoelectric effect) generating electrons which are accelerated by an electrical field toward the first of several electrodes (dynodes). The dynodes are at a positive potential relative to the photocathode with the voltage increasing from dynode to dynode by approximately 100 volts. The dynodes are coated with a material (e.g., Cs-Sb or Ag-Mg) that generates several secondary electrons for each incident electron. The electrons generated at the first dynode are accelerated toward the next dynode where electron multiplication takes place again. The multiplication process continues like an avalanche from dynode to dynode, and the resulting electron current is collected by the last electrode, the anode, to generate an electrical signal. For each electron released at the photocathode, a large number of electrons arrive at the anode. The total gain of a photomultiplier tube is k^n, where n is the number of dynodes (typically 8-14) and k the gain of a single dynode stage (typically 5). Thus the total gain is very high reaching values of 10^6 to 10^8. If dynode voltages are stable, the gain is constant and linear, providing an output signal which is

proportional to the light input from the scintillator. The gain can be adjusted by changing the supply voltage. The total voltage applied to the photomultiplier tube may be as high as 3000 volts. The voltages for the individual dynodes are usually obtained from a resistor voltage divider. Photomultipliers can produce very fast electrical pulses with a rise time of a few nanoseconds.

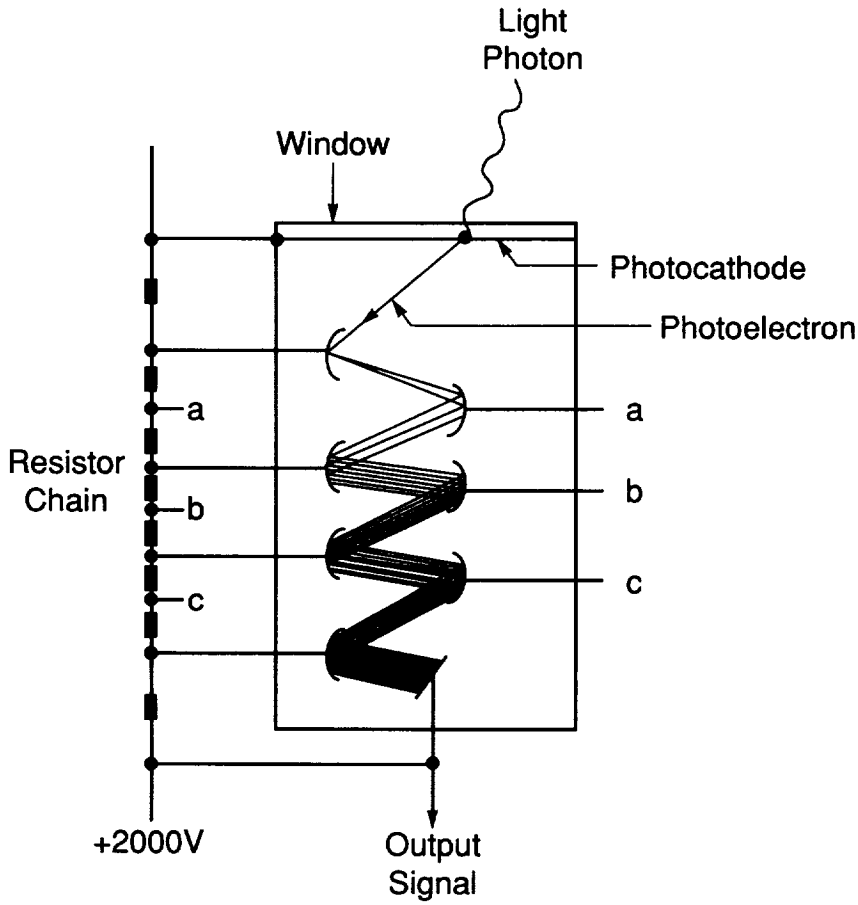

Fig. 16. Concept of a photomultiplier tube.

The spectral response of the photomultiplier (Figure 15) is determined by the type of glass used for the entrance window and the material of the photocathode (usually a low work function combination of alkali elements, K, Na, Cs). The wavelengths of the

photomultiplier peak sensitivity and the maximum light output of the scintillator material should be matched. Other performance parameters include the quantum efficiency (number of photoelectrons emitted per number of incident photons) which is 10% to 30% and the dark current in the photomultiplier (when no scintillation light is present).

E. POSITION-SENSITIVE SCINTILLATOR

Scintillators can be used as position-sensitive detectors. The amount of light collected by a PMT for a given interaction depends on the distance of the PMT from the location of the event in the crystal. As this distance increases, the light attenuation increases and the solid angle between the scintillation location and the PMT window decreases with a corresponding reduction in the amount of light collected by the PMT. In a position-sensitive scintillator detector, several PMTs (or arrays of PMTs) are coupled to the scintillator surface. By comparing the signal amplitudes of these PMTs, the location of a photon interaction can be determined (Anger camera). In the ZEBRA balloon-borne gamma ray telescope, an array of scintillator bars, with PMTs attached to both ends of each bar, provides a position-sensitive detector plane.[30] The COMPTEL gamma ray telescope uses circular scintillators with several PMTs attached at the circumference.[31,32]

F. PHOSWICH

A combination of two scintillation materials with different decay times optically coupled to a single photomultiplier is called a phoswich (phosphor sandwich) detector. The shape of the output pulse of the PMT depends on the relative light contributions from the two scintillators. By using electronic pulse shape discrimination to derive scintillation decay time components in the pulse signal, one can determine if energy deposition took place in one or in both scintillators. Phoswich scintillators are frequently used to provide active shielding against background radiation. Common phoswich combinations include NaI(Tl) with 0.23 μs and CsI(Tl) with 1.0 μs decay time or a combination of an inorganic and plastic scintillator, which usually provides much larger decay time differences.

G. ACTIVE SHIELDING

Scintillators are widely used for active shielding to discriminate against background radiation, to restrict the field of view of the primary detector (active collimation), and to improve energy resolution by negating Compton interaction, in which the scattered photon escapes from the primary detector and interacts in the shield. One or several secondary (shield) scintillation detectors, each coupled to one or several PMTs, as well as phoswich scintillators, have been used in a variety of geometrical configurations. Figure 17 illustrates typical shield arrangements. In Figure 17a, S1 is the primary scintillator (e.g., NaI(Tl)), S2 is a plastic, and S3 is another inorganic scintillator. Several photon and charged particle tracks a-e are shown. A photon entering within the field of view (track a) passes through the plastic scintillator and is absorbed in the primary detector (S1). Charged particles, entering from the field of view (track b) or from the side (track c), interact with each scintillator in their path; the resulting near simultaneous (prompt) signals are rejected by anticoincidence circuits (anticoincidence shield). A photon (track d), entering through the side, is absorbed in shield scintillator S3. Track e represents a photon scattered in S1 and absorbed in S3. The event is rejected by an anticoincidence circuit (it is an undesirable event because of partial energy deposition in S1). The field of view is determined by the geometry of S1 and S3. An alternate method of active collimation is an inorganic scintillator with holes, positioned in front of the primary detector as indicated in Figure 17b, which shows also a phoswich charged particle shield. S1 and S2 is a combination of an inorganic and a plastic scintillator viewed by the primary detector PMT. Charged particles which interact with both scintillators are detected by pulse shape discrimination and are rejected.

H. DETECTOR RESPONSE

Not all of the incident photon energy is necessarily deposited in the detector. Depending on photon energy, angle of incidence, and the interaction process, a portion of this energy may be lost. Therefore, the pulse height spectrum obtained from a detector is not a true representation of the source spectrum and needs to be corrected with the detector's response function. This function is generated from a combination of calibration measurements with radioactive sources and calculations using Monte Carlo simula-

tions which include the detector geometry, background radiation environment, detector shielding, and detector response to source flux and background radiation.

Scintillation detectors in various configurations have been flown on balloons, rockets, and satellites. Examples of two more recent applications are given below.

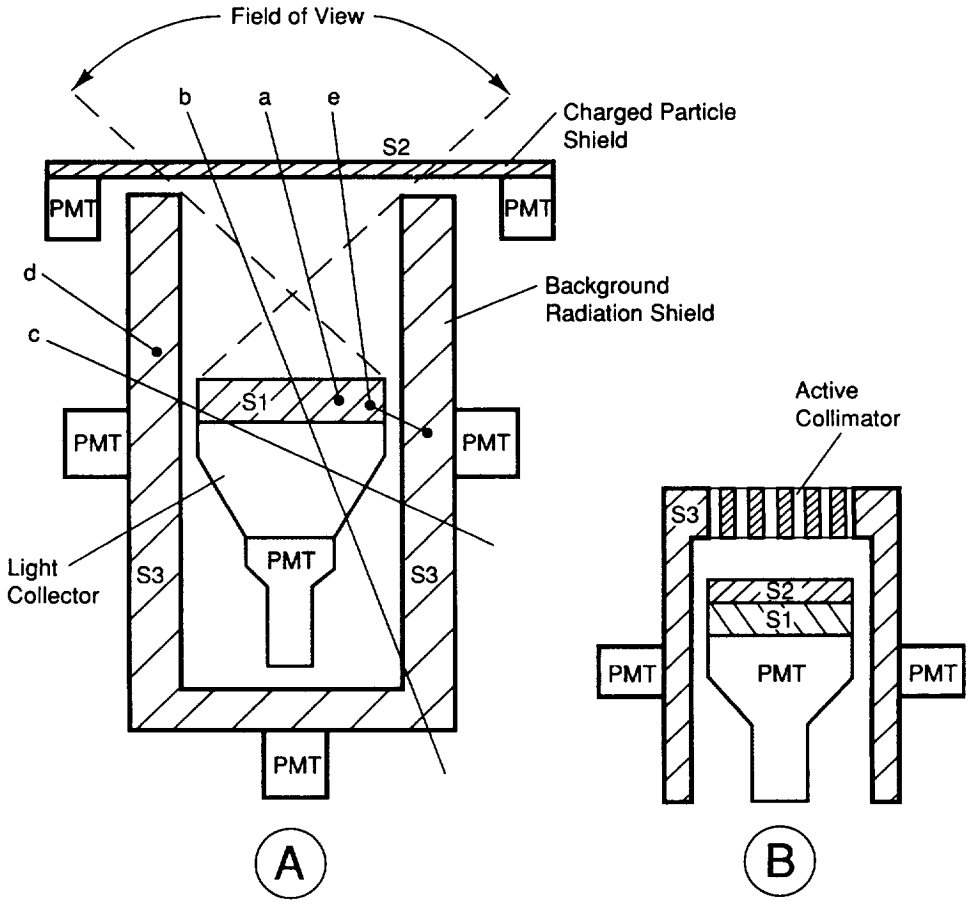

Fig. 17. Scintillation detector concept. Shown are two approaches to shielding using secondary scintillators (S2, S3). S1 is the primary detector. Several photon and charged particle tracks (a-e) are indicated in Figure 17a.

X-Ray and Gamma Ray Astronomy Detectors

1. BATSE Detector

The Burst and Transient Source Experiment (BATSE) is one of four experiments on the Compton Gamma Ray Observatory, launched in 1991, to study astronomical gamma rays sources. BATSE was designed to detect and locate gamma ray bursts (which occur at seemingly random times and locations in the sky), to analyze their spectral and temporal characteristics, and to investigate other transient sources.[33] The experiment consists of eight identical detector modules (Figure 18) attached to the corners of the observatory to provide a full sky view (except for the portion obstructed by the Earth). Each detector module contains a thin, large-area scintillation detector for high time resolution studies, which is optimized for sensitivity and angular

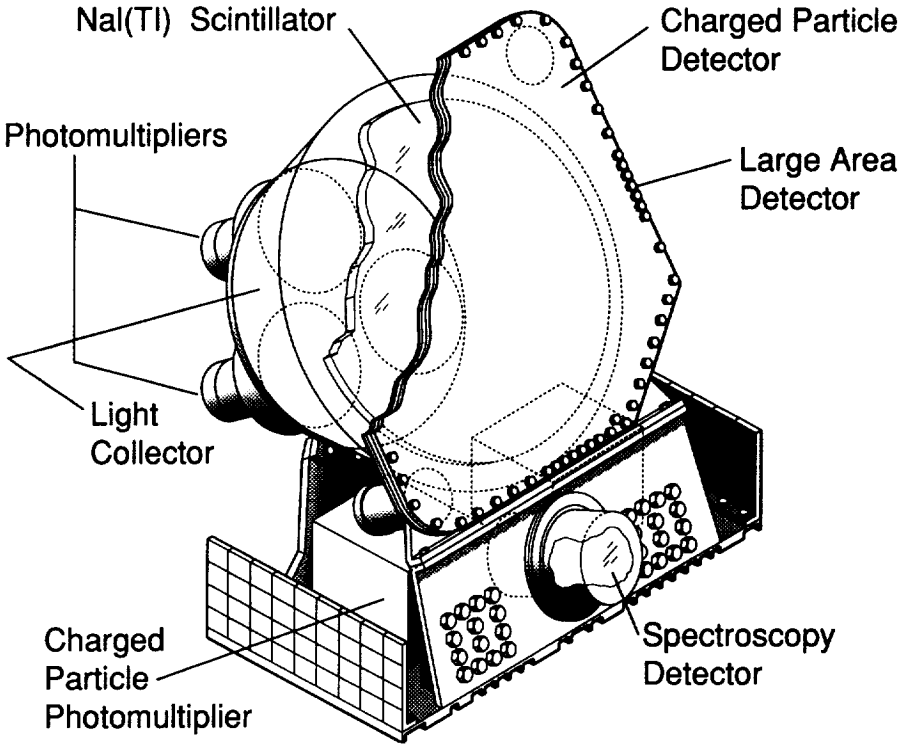

Fig. 18. BATSE detector module. The BATSE detector module contains two detectors, a large-area scintillator and a smaller spectroscopy scintillator.

response, and a thicker spectroscopy scintillation detector to increase the energy range and provide better spectral resolution (Table 6). Their combined energy range is 15 keV to over 100 MeV.

The large-area detector contains a NaI(Tl) crystal scintillator, hermetically sealed in a housing which is attached to a light collector cone. Scintillation light is detected by three photomultiplier tubes (each 12.7 cm in diameter) inserted into the rear surface of the light collector. Their output signals are added together. Passive shielding of the rear hemisphere of the detector is provided by the light collector housing, which is lined on the inside with a layer of lead and tin. (The tin layer absorbs K-shell x-rays generated in the lead foil.) This shielding is very effective for gamma ray energies up to 300 keV. A highly reflective barium sulfide ($BaSO_4$) paint is applied to the inside of the light collector. The front face and edge of the NaI crystal are covered with white paper providing diffuse reflection of the scintillation light back into the light collector. The scintillator enclosure consists of a thin aluminum window in front of the scintillator and a fused quartz window with an optical coupling layer facing the light collector. A plastic scintillator, which covers the front of the NaI(Tl) scintillator housing, provides an active shield against charged particles. Two PMTs are coupled to the plastic detector by Lucite light guides. Diffuse cosmic x-rays (below 20 keV) which pass through the charged particle detector, are absorbed in the aluminum window of the NaI(Tl) crystal housing.

The spectroscopy detector (Figure 19) is mounted below the large-area detector. It contains a NaI(Tl) scintillator crystal coupled directly to the photomultiplier window. Passive shielding of the detector is provided by the aluminum housing with a lead/tin lining similar to that of the large-area detector. A thin beryllium window permits observations of low-energy photons (down to 15 keV). Because of its smaller diameter, the spectroscopy detector has a lower sensitivity than the large-area detector but it has a better energy resolution because of its thicker crystal directly coupled to the PMT window. Its angular response is almost isotropic.

The large diameter-to-thickness ratio of the large-area detectors results in an angular response pattern which is similar to that of a cosine function for energies below 300 keV where the scintillator is opaque to the incident photons. At higher energies, the response becomes flatter than a cosine function. The combined surface of the eight large-area detectors forms a regular octahedron. A gamma ray burst is always seen simultaneously by four detectors and its location on the sky can be determined from

the count rates of these detectors and the known angular response of each detector module. The angular resolution for burst location is approximately 2° for strong bursts.

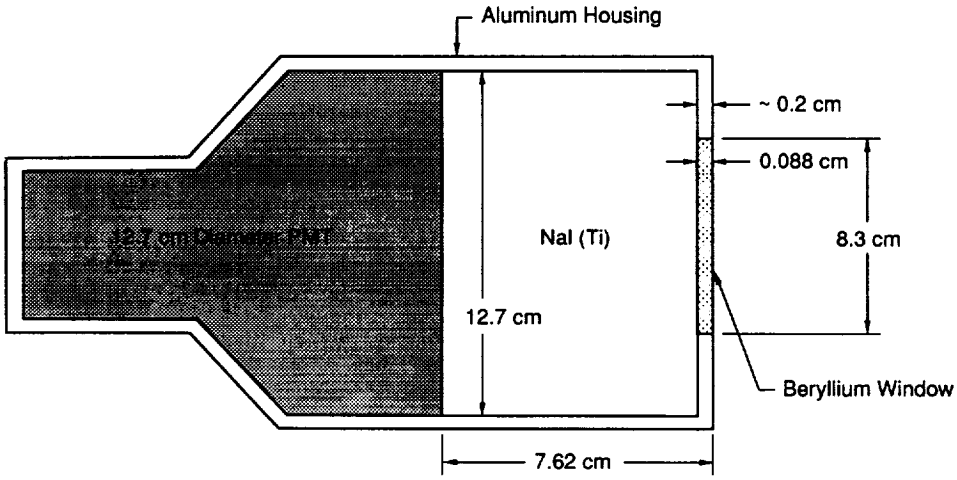

Fig. 19. BATSE spectroscopy detector.

When the gamma ray flux in two or more detectors exceeds a preset threshold, the burst mode is triggered which records data at a high rate with high time resolution. Gamma ray bursts are short transient events with a typical duration of several ms to a few hundred seconds. BATSE can record large amounts of data in a short time with a time resolution of 64 ms to study fast gamma ray flux variations. Characteristic data of the BATSE detectors are given in Table 6.

Table 6. BATSE Detector Characteristics

	Large-Area Detector	Spectroscopy
Material	NaI(Tl)	NaI(Tl)
Area	2,015 cm^2	127 cm^2
Diameter	50.8 cm	12.7 cm
Thickness	1.27 cm	7.62 cm
Energy Range	30 keV to 2 MeV	15 keV to 110 MeV
Energy Resolution	27% at 88 keV	7.2% at 662 keV

2. COMPTEL Telescope

COMPTEL is another one of the four experiments on the Compton Gamma Ray Observatory which was launched in 1991. It is an imaging Compton telescope for gamma rays in the MeV region.[31,32] Compton scattering of the incident photon is used to measure its original energy and direction of motion. The instrument has two planes of detector arrays, separated by 150 cm, each array consisting of several individual detectors (Figure 20). An incoming gamma ray photon is scattered first in passing through a detector in the forward plane and is absorbed in one of the second plane detectors. The scatter angle ϕ of the incident photon is obtained from the energy deposition in the detectors: ϕ = arc cos [1 - ε/E2 + ε/(E1 + E2)], where e is the restmass of the electron and E1 and E2 is the energy deposited in the forward and rear detector. Measurements of the energy loss E1 and E2 together with measurements of the event position in each detector plane establish a cone for possible directions to the source, which becomes an annulus on the sky when measurement uncertainties are included. The source position is determined from the intersections of these rings obtained from many measurements.

All detectors are position-sensitive scintillators which measure the location of the photon interaction with an uncertainty of less than 0.5 cm by comparing the pulse signal amplitudes of several PMTs attached to each scintillator. In the forward detector plane, seven scintillation detectors containing an organic liquid (NE213A), which has low density and low Z number to reduce multiple scattering, are used to measure deposited energy and interaction position. Each detector's scintillator cell is viewed by eight PMTs located around the circumference of the cell. In the second (rear) detector plane, 14 position-sensitive NaI scintillation detectors are used to measure again the deposited energy and interaction position of the scattered photons. Each of these detectors is viewed by seven PMTs attached to the lower face of the scintillator. The angular resolution of the telescope depends on the energy resolution of the detectors and the uncertainty in the event positions.

By measuring the time of flight between the two detector planes (5 ns light travel time), the instrument can discriminate against background caused by other interaction events or gamma rays arriving from outside the field of view. Pulse shape discrimination in the liquid scintillators is used for additional background suppression.

Each detector plane is completely enclosed in a plastic (Ne110) scintillator which provides a charged particle shield with little attenuation of the incident gamma ray flux. The plastic shields are viewed by a total of 96 PMTs. Characteristic data of the COMPTEL telescope are listed in Table 7.

Table 7. COMPTEL Instrument Characteristics

Energy Range	0.8-30 MeV
Energy Resolution	5%-10%
Angular Resolution	2° (1 σ)*
Upper Plane Detectors (7)	Liquid scintillators, 28 cm dia., 8.5 cm thick, total area = 4310 cm^2
Lower Plane Detectors (14)	NaI, 28 cm dia., 8.5 cm thick, total area = 8620 cm^2

*energy dependent

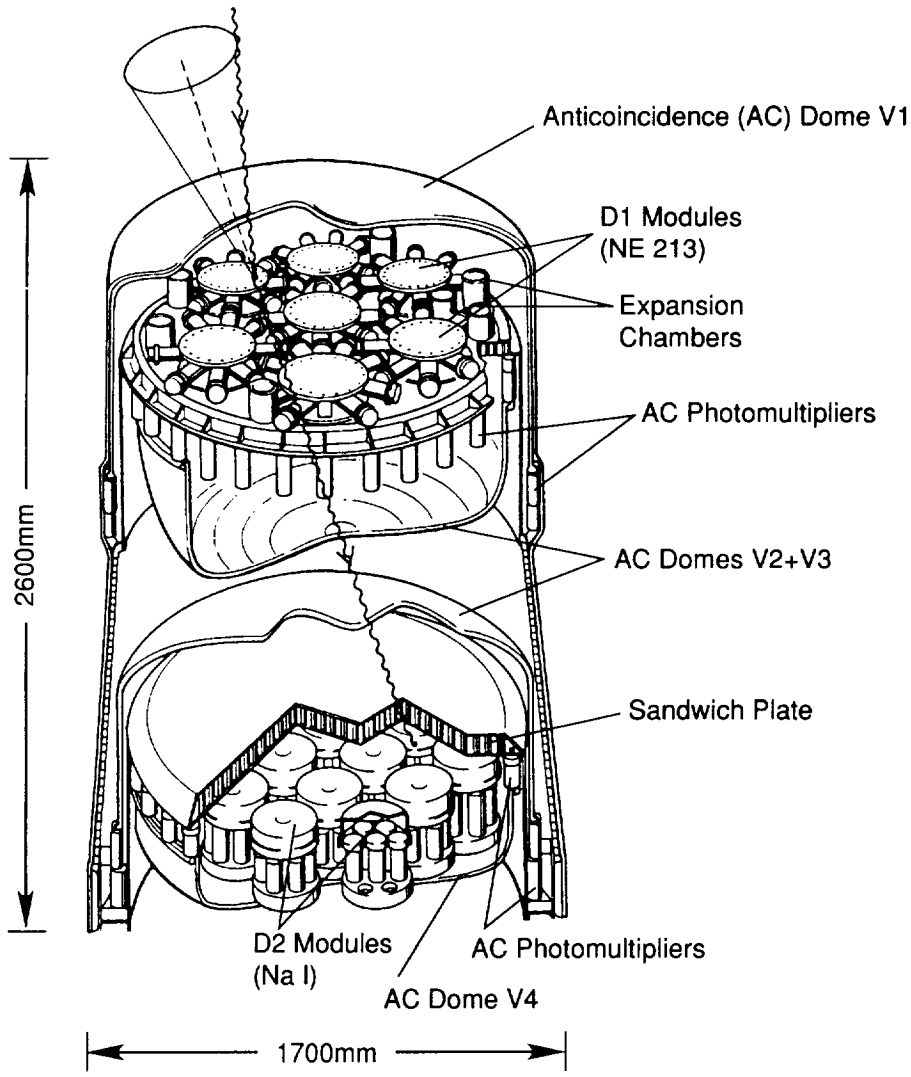

Fig. 20. COMPTEL gamma ray telescope (courtesy Max Planck Institute for Extraterrestrial Physics).

X-Ray and Gamma Ray Astronomy Detectors

V. MICROCHANNEL PLATES

A variant of the photomultiplier tubes discussed in section IV.D is the channel electron multiplier.[5] This device can be looked on as a photomultiplier tube with a continuous dynode running its entire length when operated in a vacuum. Electrons liberated at the front end of the channel multiplier, through the interaction of incident x-ray photons, are accelerated down the tube by the applied potential, repeatedly striking the specially-coated tube walls. Each hit generates several secondary electrons which also are accelerated down the tube and, in turn, produce further electrons of their own as shown in Figure 21. In this manner a cascade of electrons is produced which eventually emerges from the end of the multiplier tube.

Large numbers of these channels can be bundled together to form a microchannel plate (MCP), with each channel still acting as an independent multiplier (Figure 21). Typical plates have individual channels of diameter 12.5-25 μm and areas of 10-100 cm^2. They are formed by taking a hollow rod of lead glass (glass containing up to 50% by weight of lead oxide) and inserting a core of etchable material, usually another type of glass. The assembly is then drawn to produce a fiber of order 1 mm diameter, and these are then cut and stacked to form a bundle of hexagonal cross section. Individual bundles are then further stacked and drawn and heated in an oven to fuse the assembly, which is cut and polished to the desired configuration. The final step is to etch away the channel interiors and deposit contact electrodes and a suitable channel coating to ensure a high secondary electron yield for charge multiplication.[6]

In operation, very large gains are possible with the MCP provided steps are taken to minimize positive ion feedback. This is caused by residual gas atoms in the channels being ionized by the avalanche and then traveling back up the channel where they can initiate large after-pulses through collisions with the walls. The simplest way to avoid this is to not let the ions "see" back to the start of the channel, where they would have a maximum effect, and this is usually accomplished by utilizing two plates in a chevron configuration with a small (~1 mm) gap in between, as shown in Figure 21. Here the plates are biased at an angle of order 15° with respect to each other. A second, though not so widely-used technique is to employ curved microchannel plates. With positive ion feed-back controlled in this manner, gains of greater than 10^7 are possible before saturation sets in. This saturation occurs when the avalanche depletes the charge from the

channel walls and it cannot be replaced on the time scale of the event. This effect also sets the maximum count rate that the device can handle.[6]

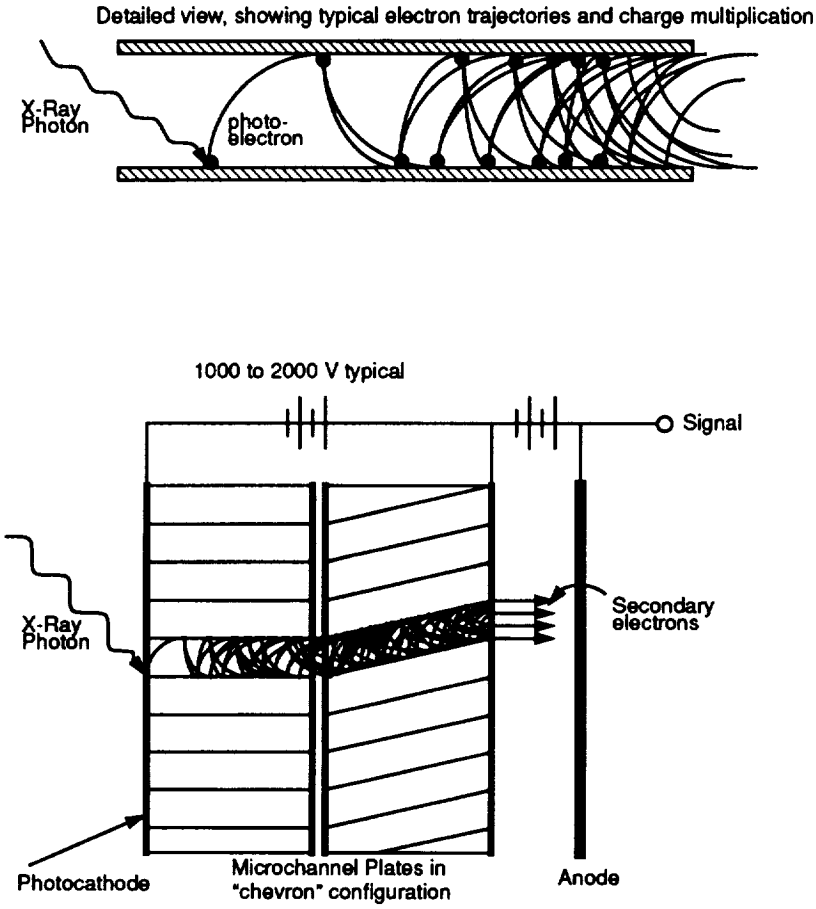

Fig. 21. Schematic of the operation of a microchannel plate system.

Microchannel plates have been used at the focus of x-ray telescopes to provide high resolution imaging. For enhanced response in the soft x-ray region, the front surface of the plate is usually coated with a material having a high electron yield, such as magnesium fluoride. This was the case for both the high resolution imager (HRI) on the Einstein satellite[34] and for the channel multiplier array on EXOSAT.[35] More recently, cesium

iodide has been found to offer further enhancements in quantum efficiency, and this material was used for the microchannel plate at the heart of both the ROSAT HRI and wide field camera (WFC).[18] Quantum efficiencies as high as 30%-40% are possible for cesium iodide coated plates compared with only a few percent for uncoated ones. This efficiency is dependent upon incident photon angle though, and approaches zero at normal incidence and at the grazing angle where the incident x-ray is reflected rather than absorbed in the channel coating.

Even when operated below the saturation limit the microchannel plate has little or no energy resolution. With cesium iodide coating the output signal is dependent upon the magnitude of the incident photon energy, but the spread in signal sizes for a monoenergetic input is so large that nothing more than two or three energy bins are possible over a typical 10-20 keV energy band. The usual course of action is to include moveable filters in front of the microchannel plate to select the energy range of interest.

The principal attraction of the MCP is its extremely high spatial resolution which is particularly desirable at the focus of an x-ray telescope. Thus the MCP has so far been used at low x-ray energies <10-20 keV even though it is potentially useful up to hundreds of keV. At low energies the x-rays penetrate only single-channel cells, and the resulting spatial resolution can be on the order of the channel size themselves, i.e., tens of microns. To achieve this resolution several different readout schemes have been employed. For the Einstein and ROSAT HRIs, a system of crossed grids connected to amplifiers measured the centroid of the charge cloud exciting the MCP, whereas, for the ROSAT WFC, a resistive disc was used. Here, the charge signal was registered by four amplifiers located around the periphery of a resistive collection electrode. By taking suitable ratios of the signals, which are modified by the distributed resistance between the collection site and each amplifier, the position can be determined with high precision. The resulting spatial resolutions were 33 μm and 20 μm FWHM, respectively, for the Einstein and ROSAT HRIs and 100 μm FWHM for the ROSAT WFC (see reference [6] and references therein for a more detailed account of position sensing techniques).

The largest MCP under construction for x-ray astronomy is that for the high resolution imaging camera (HRC-I) intended for the AXAF-I mission[36] which is currently scheduled for launch in 1998. This device has linear dimensions of 10 cm x 10 cm, a pore size of 12.5 μm, and utilizes a crossed grid readout with 65 amplifiers per axis to determine the charge centroid to an ac-

curacy of better than 25 μm. Full details of the HRC are given in Table 8.

Table 8. Details of the Proposed AXAF Imaging High Resolution Camera (HRC-I)

Configuration	Chevron pair, 6° bias front, 6° bias rear, 50 μm gap between plates
Area	10 cm x 10 cm
Geometry	12.5 μm pixels, 15 μm pitch
Photocathode	Cesium iodide
Readout	Crossed grids, 65 x 65 preamplifiers
Spatial Resolution	Better than 25 μm FWHM
Time Resolution	16 μsec
Background Rate (Low Noise Glass)	6×10^{-3} counts/cm^2 sec (internal)
Bandwidth	0.1 to 10 keV

Finally, in order that they can provide the highest sensitivities for x-ray astronomy, the MCPs must have extremely low backgrounds. Early work showed that most MCPs had a common background level regardless of the specific details of the instrument and this was later found to be due to radioactivity, in particular K^{40}, in the glass used for the construction.[37] A development program is currently underway to produce low background plates for use in future missions such as AXAF.

VI. SEMICONDUCTOR DETECTORS

A. INTRODUCTION

The advantage of semiconductors over other solid materials for detecting radiation is the ease with which information carriers, in this case electrons and holes, can be formed by the absorption of radiation.[5] Semiconductors are crystalline materials distinguished from metals by an energy band structure consisting of three regions: the valence band, the forbidden gap, and the conduction band (Figure 22). The valence band is the lowest energy band and is filled with bound electrons which are unable to drift through the crystal. The forbidden gap spans the range of electron energies forbidden by quantum mechanics. The conduction band corresponds to the energies of electrons which are free to move throughout the crystal lattice. The difference in energy between the lowest energy electron in the conduction band and the highest energy electron in the valence band is called the bandgap E_g. The bandgap is the most important parameter in semiconductor physics. For a semiconductor, E_g is typically about 1 eV. Equation (4) gives the number density of thermally-generated electron-hole pairs as a function of the bandgap energy

$$n = CT^{3/2} \exp(-E_g/2kT), \tag{4}$$

where C is a proportionality constant that depends on the material, T is the temperature in Kelvin, E_g is the bandgap energy, and k is the Boltzmann constant. In semiconductors at room temperature some electrons in the valence band can be thermally excited into the conduction band and the conduction band is partially filled. Insulators have bandgaps larger than 5 eV and have an empty conduction band.

A material in which electrons are majority charge carriers is designated n-type; if holes are the majority carriers, the material is p-type. A hole is a vacancy formed when an electron in the valence band is excited into the conduction band. An electron-hole pair is the solid state analog of an ion pair produced in a gas-filled ionization chamber. When a photon is photoelectrically absorbed in a semiconductor, the ejected photoelectron loses approximately two-thirds of its energy as heat and the remainder goes into the formation of electron-hole pairs. The short photoelectron pathlengths in solids makes possible quite good spatial

resolutions: ~250 μm for a 30-keV x-ray in Ge. The energy required to form an electron-hole pair (2-5 eV) is approximately 3 times the bandgap energy; this compares favorably with energies in excess of 20 eV required to form ion pairs in gases. The Fano factors for gases and semiconductors are of comparable magnitude (~0.1). Thus the small amount of energy required to produce electron-hole pairs in solid state detectors translates into potentially better energy resolution than any other detector technology with the exception of calorimeters (described in section VII). For a typical semiconductor, one would ideally expect an energy resolution of approximately 200 eV (FWHM) at 20 keV. Since semiconductor detectors are not amplifying devices like proportional counters, energy resolution is degraded by the noise from the amplifying electronics. Further noise comes from system capacitance and fluctuations in the leakage current flowing through the detector (shot noise). Also, imperfect charge collection (discussed below) will further degrade the energy resolution.

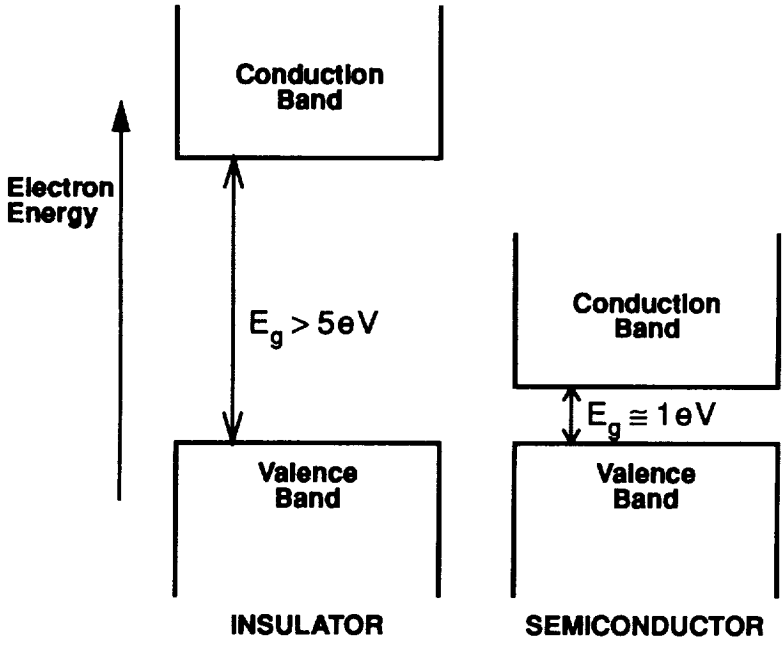

Fig. 22. Illustration of the band structure for insulators and semiconductors.

Semiconductor Detectors

At the present time, Si and Ge are the materials most often used in semiconductor detectors for x-ray and gamma ray astronomy. Unfortunately, as a result of their narrow band gaps, these materials must be kept at low temperatures to reduce thermally generated noise. Since refrigeration equipment tends to be heavy and bulky, and hence, expensive to put on a spacecraft, semiconductors with bandgaps sufficiently large to operate at room temperature are much sought after. For hard x-ray and gamma ray spectroscopy, it is important to find semiconducting material with high values of Z (atomic number). A high value of Z is desired to ensure a high photoelectric cross section so that all the incident energy is likely to be absorbed in the detector. For example, in the case of Si, the Compton cross section exceeds the photoelectric cross section for energies above 50 keV; a high background from Compton scatters makes it difficult to make a precise energy measurement. HgI_2 and CdTe are two materials which have attracted a great deal of interest since the 1970s. Work on these two materials has continued up to the present time, but progress has been slow due to their limited applications outside x-ray and gamma ray detector technology. The major hurdle has been to produce high quality crystals having good charge transport properties (measured as the mobility lifetime product for electrons, $\mu_e\tau$). The mobility-lifetime product is a measure of how efficiently charges in a semiconductor can be collected at an electrical contact. Unless the detector is kept very thin, a small value of $\mu_e\tau$ means that charges will be lost enroute to their collection point, and energy resolution, which depends on the number of charges collected, will be poor. As seen in Table 9, CdTe and HgI_2 have small values of $\mu_e\tau$ compared to both Si and Ge; fortunately, the former have sufficiently large bandgaps which allow room temperature operation. For some applications, the convenience of not refrigerating the detector combined with high absorption efficiency more than compensates for inferior energy resolution.

Table 9. Important Physical Properties of Some Semiconducting Materials Used in X-Ray and Gamma Ray Detectors

Semiconductor	Atomic #(s)	$\mu_e\tau$ ($cm^2\ v^{-1}$)	Bandgap (eV)	Fano Factor (typ. values)	Energy per Electron-Hole Pair (eV)
Si	14	$>10^{-1}$	1.12	0.1 [38]	3.61
Ge	32	$>10^{-1}$	0.74	0.08[38]	2.98
HgI_2	80, 53	$<10^{-4}$	2.13	0.20[39]	4.22
CdTe	48, 52	$<10^{-3}$	1.47	---	4.42

B. Semiconductor Detector Types

1. Slab with Ohmic Contacts

The simplest radiation detector made from a semiconducting material would consist of a slab of semiconductor with metallic contacts deposited on opposite faces of the material (Figure 23). The metal contacts simply provide electrical connection to the semiconductor and are called ohmic contacts. If a potential is applied to such a device, electrons and holes liberated by absorbed radiation would drift to opposite contacts and the collected charge would be proportional to the energy absorbed. Such a device would be a direct semiconductor analog to a gaseous ionization chamber.

Because of its large bandgap (2.1 eV), HgI_2 benefits from very low leakage current at room temperatures, so detectors made from this material take the form described above. Up to now, HgI_2 is the only semiconductor other than Si and Ge known to be used for x-ray astronomy. The balloon experiment of Ogawara et al.,[40] flown in 1980, used a detector containing eleven HgI_2 crystals to detect radiation from the black hole candidate Cyg X-1 (see Table 10). Hoping that an HgI_2 detector would one day be put at the focus of a hard x-ray concentrator, some members of this team later demonstrated how the high photoelectric cross section of HgI_2 makes possible the construction of a compact, highly absorbing detector which will have reduced background and hence be more sensitive than a detector made from lower Z materials. During a balloon flight in 1982, they found that the background rate was a factor of 5 times lower than with NaI/CsI or Ge systems having similar efficiency in an energy range of 40-80 keV.[41]

Table 10. Characteristics of the HgI_2 Detector Flown Aboard the Balloon Experiment of Ogawara, et al.[40]

Area	7.6 cm^2
Crystal Thickness	750 μm
Absorption Efficiency	~50% @ 100 keV
Energy Range	20 to 100 keV
Energy Resolution	between 2 and 6 keV @ 60 keV

2. PN Junctions

Unfortunately, for common semiconductors like silicon and germanium with a relatively low resistivity, a detector simply consisting of a slab with ohmic contacts would suffer from excessive shot noise. Shot noise is the noise resulting from fluctuations in charge collected from the leakage current during the measuring time of the signal processing electronics.

To significantly reduce the leakage current, a diode can be made from an intrinsically n-type or p-type material by having one face doped with an impurity to form a p-type or n-type layer, respectively (Figure 23). When reverse biased, the PN junction provides high resistance to current flow and hence very little leakage current. Equilibrium between carrier diffusion and internal electric fields will produce a high resistivity region called the depletion region. The depletion region corresponds to the sensitive depth of a semiconducting detector. The size of the depletion region, d, is proportional to the square root of the product of the resistivity, ρ, of the semiconductor and the voltage applied across the junction, V.

$$d \cong (2\varepsilon V \mu \rho)^{1/2}, \tag{5}$$

where ε is the dielectric constant and μ is the mobility of the majority carriers. By increasing the voltage, the depletion region can be increased until it extends fully through the semiconductor, i.e., the detector is fully depleted or until the breakdown voltage for the semiconductor has been reached.

3. PIN Detectors

For silicon with the highest currently available purity, the maximum depletion depth attainable is 1-2 mm before breakdown

occurs. One can see from equation (5) that the voltage required to achieve a desired depletion depth is inversely proportional to the resistivity of the semiconductor. To increase the maximum obtainable depletion depth of a semiconductor detector, an alkali metal such as lithium is diffused through high purity silicon or germanium to neutralize excess charge carriers and create a region of intrinsically high resistivity; i.e., the semiconductor has been compensated. Lithium drifted silicon and germanium are referred to as Si(Li) and Ge(Li), respectively. A so-called intrinsic semiconductor is one in which all or (practically all) charge carriers in the conduction band are produced by thermal excitation [see equation (4)]. The diffusion process naturally forms what is called a PIN (p-type-intrinsic-n-type) detector (Figure 23). The face of the material in contact with the lithium becomes heavily doped n-type (represented by n^+) and can act as an electrical contact. The bulk of the semiconductor has a uniform concentration of lithium atoms which mop up excess holes resulting in very few charge carriers; this region acts as though it were intrinsic. The uncompensated face of the detector is p-type and is often coated with metal to form an ohmic contact. The PIN detector is reverse biased as is the PN diode with the intrinsic region determining the sensitive volume of the detector.

The Broad Band X-Ray Telescope (BBXRT) which flew aboard the Space Shuttle *Columbia* in 1990 used nested, conical mirrors to focus x-rays on a segmented Si(Li) detector having five elements (Figure 24). Segmentation was achieved by cutting grooves into the face of a monolithic Si(Li) diode. By subdividing a large, 3 cm diameter diode, better energy resolution was achieved through the reduction of capacitance. Segmentation also provided spatial information unavailable from single pixel detectors. The detector characteristics are summarized in Table 11. When observing weak point sources, background was suppressed by rejecting events having inner and outer pixel coincidences.[42]

Table 11. Physical Characteristics of the Detector Used on BBXRT

Detector Type	Segmented Si(Li)
Area	28 cm^2
Energy Range	0.5 to 12.0 keV
Energy Resolution	~185 eV @ 5.89 keV

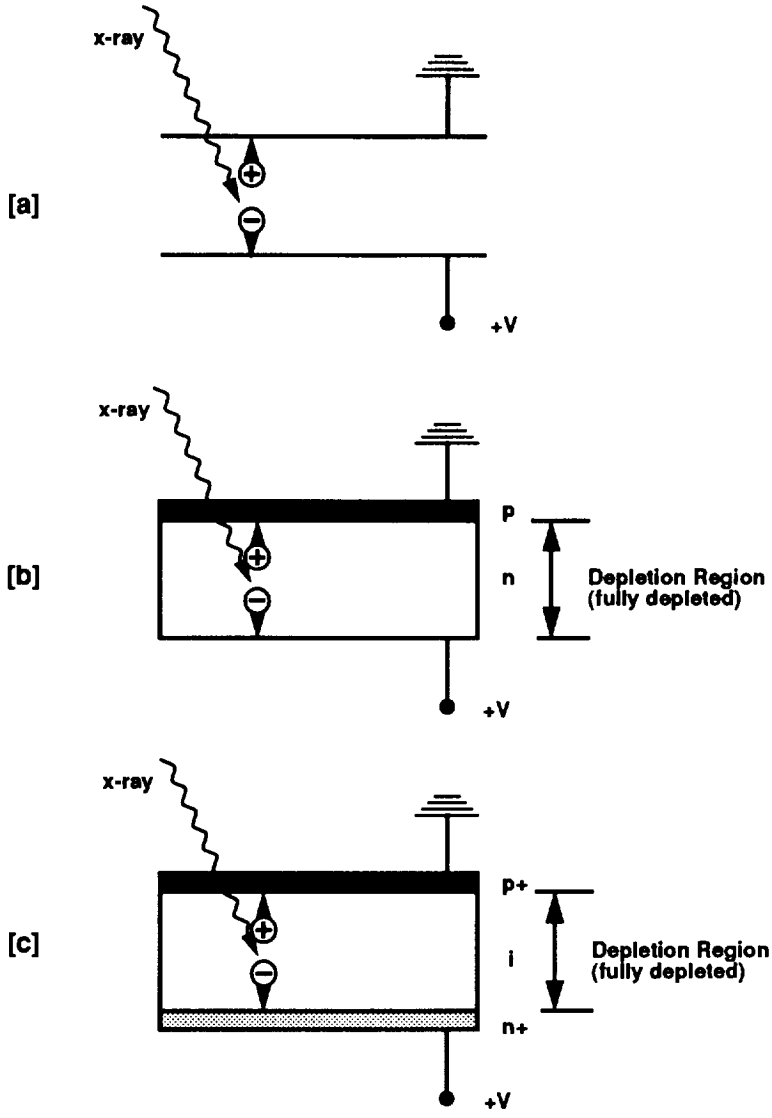

Fig. 23. (a) Slab with ohmic contacts, (b) PN junction, and (c) PIN diode detector.

Because of the high mobility of lithium in silicon and germanium detectors, the lithium ions gradually redistribute themselves due to internal electric fields. In germanium the mobility of lithium is sufficiently high to require that Ge(Li) detectors be

kept at liquid nitrogen temperature (77 K) at all times to avoid decompensation. Si(Li) detectors can be kept at room temperature for short times without deleterious effects. Apart from the need to avoid lithium redistribution, Si(Li) and Ge(Li) detectors are kept at liquid nitrogen temperatures during operation to improve energy resolution by reducing leakage current. Because of its extreme instability at room temperature, Ge(Li) has been supplanted in recent years by high purity germanium (HPGe) which is sufficiently pure to form detectors having equivalent sensitive volumes to its unstable predecessor.

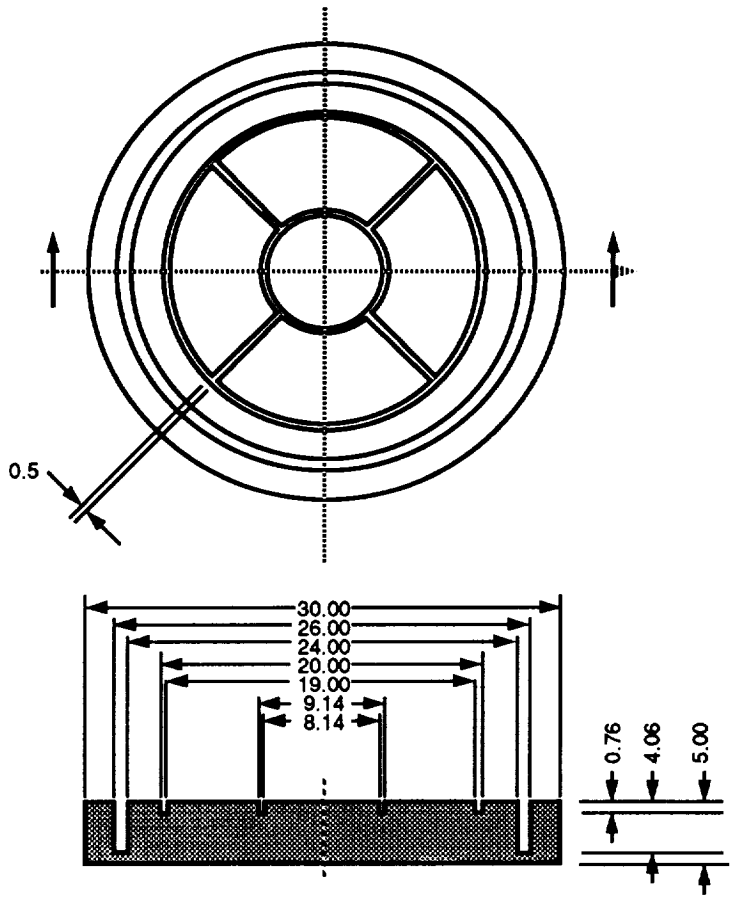

Fig. 24. Segmented Si(Li) detector for the Broad Band X-Ray Telescope (BBXRT).

The Gamma Ray Imaging Spectrometer (GRIS) observed supernova SN 1987A during April and October 1988.[43] The balloon-borne detector consisted of an array of seven HPGe cylindrical detectors. For imaging, a coded aperture mask has been built but not yet flown with the detector. GRIS was flown again in April and May of 1992 from Alice Springs, Australia. For this flight, the Ge detectors were replaced with isotopically enriched ^{70}Ge cylinders which, having a low cross section for neutron activation, suppressed background by a factor of 2.[44] (For a summary of GRIS properties, refer to Table 12.) A spectrometer similar to GRIS but containing nine detectors is included in a plan for the European Space Agency's INTErnational Gamma Ray Astrophysics Laboratory (INTEGRAL).

Table 12. Physical Characteristics of the Detectors Used on GRIS

Detector Type	HPGe (96% ^{70}Ge)
Area	242 cm^2
Energy Range	15 keV to 10 MeV
Energy Resolution	~2 keV @ 1 MeV

At least one group, in Italy, is studying the properties of two-dimensional arrays of CdTe detectors for astronomy.[45] To achieve high absorption efficiency while maintaining reasonable energy resolution (2% at 511 keV), rectangular bars of CdTe (2 x 2 x 10 mm) are oriented so that incident radiation is absorbed along their long dimension and are biased so that the applied electric field is along the small dimension of each bar. In the future, this group plans to expand their current array of five diodes to construct a large-area detector to image cosmic sources of the electron-positron annihilation line at 511 keV.

4. CCDs

A charge coupled device (CCD) is a solid state imaging device which typically consists of a closely-spaced array of MOS (metal-oxide semiconductors) capacitors formed by sandwiching an insulating oxide layer between a heavily doped region of semiconductor (p-type silicon) and a metal electrode (Figure 25). Positive bias is applied to all electrodes to produce surface depletion. Electrons generated by photoelectric absorption of x-rays in the semiconductor are stored until an increasing applied voltage on an adjacent electrode forms a deeper potential well and electrons

are transferred to that electrode. By continuing this process, charges are transferred from pixel to pixel until the entire device is read out.[46]

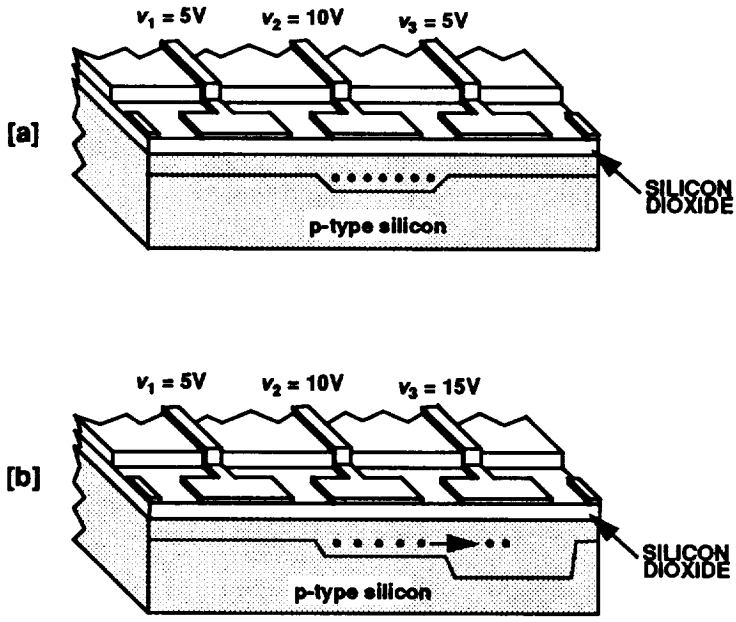

Fig. 25. Diagram illustrating how charge is transferred in a three-phase charge coupled device. (a) Electrons lie in the potential well formed by high voltage on v_2. (b) Increased voltage on v_3 causes charge to be transferred to the lower potential region.

The AXAF CCD Imaging Spectrometer (ACIS) will be a core focal plane instrument for AXAF-I. ACIS will consist of two CCD arrays: a two-dimensional imaging array and a linear array for spectroscopy. The imaging array will have four CCDs and will cover 295 square arc minutes on the sky. To provide almost seamless coverage of the whole image, the CCDs are each read out from only one side; hence, they are abuttable on three sides. The spectroscopic linear array will likely consist of six CCDs which will be used to separate orders in a spectrum produced by a grating.[47] (For a summary of the ACIS CCDs, see Table 13.)

High resistivity silicon (10,000 Ohm-cm) allows the CCDs to be depleted to a depth of 50 μm which will give a high detection efficiency in AXAF's energy band; at 5.9 keV, for example, ACIS will absorb 80% of the incident x-rays. Many cosmic ray particles

produce large signal pulses across many pixels because of their high energies and long pathlengths in silicon. By rejecting such multi-pixel events, more than 99% of the cosmic ray background can be eliminated. The combination of gratings and CCD will yield an energy resolution 10 times better than the CCD alone.

Table 13. Parameters of ACIS CCDs

Number of Pixels	1024 x 1024
Pixel Size	25 x 25 μm^2
Time Resolution	54 μsec to 6 msec
Energy Range	0.1 to 10 keV
Energy Resolution	140 eV @ 5.9 keV

Radiation damage from charged particle bombardment in space increases the number of carrier trapping sites in silicon which results in a loss of electrons during readout. Annealing at ~100 °C for a number of hours removes much of the radiation damage. Low temperature operation (through passive cooling in space) can improve charge collection efficiency significantly. To minimize the effects of radiation damage, the CCDs are divided into parallel strips, 512 pixels wide and 1024 pixels long with an amplifier attached to both ends of the 512 pixel serial register. Half an image will be read out on the left side of the register and the other half will be read out on the right side. This readout scheme reduces the distance charge must be transferred and thus makes the CCD less susceptible to radiation damage.[48]

VII. CALORIMETERS

Calorimeters measure energy through the accompanying temperature rise in a suitable absorber. This technique has long been used in nuclear physics to record the energy from radioactive decays and has found widespread use in infrared astronomy where liquid helium cooled bolometers are used to record the thermal emission from cosmic sources. The radical departure for x-ray astronomy is that the device must measure individual photons rather than a continuous flux and thus the temperature rise associated with the absorption of a single x-ray photon must be registered with accuracy.

It can be quickly shown that this technique has the potential for remarkably good energy resolution limited, in an *ideal* case, only by thermodynamic energy fluctuations within the absorber which represent a background against which the temperature rise from the absorbed event must be measured (from reference [49]). Simple statistical calculations give this limiting resolution as

$$\Delta E = 2.36(kT^2C)^{0.5}, \qquad (6)$$

where k is Boltzmann's constant, T is the detector temperature, and C is the detector thermal capacity. A small piece of silicon 0.5 mm square and 25 μm thick has a heat capacity of 4×10^{-15} JK^{-1} at 0.1 K, giving $\Delta E < 1$ eV (FWHM). This should be compared with a theoretical limit of around 200 eV for a conventional solid state detector (section VI). At 6 keV the absorption efficiency of the above absorber would be greater than 50% and thus a calorimeter operating at a fraction of a degree Kelvin offers the potential of an instrument combining high quantum efficiency with the ultra-high energy resolution of a dispersive spectrometer such as a Bragg crystal or diffraction grating.

The principal components of a calorimeter are an absorber to convert the incident photon energy to heat, a thermometer to measure the resulting temperature rise and a thermal link to cool the absorber after the event has been registered. A schematic of a typical calorimeter is shown in Figure 26.

The absorber must ideally convert all of the incident photon energy to heat. The temperature rise of the absorber is then given by the absorbed energy divided by the thermal capacity of the device. For maximum sensitivity the thermal capacity must be kept at a minimum and this, in turn, necessitates the use of special materials and very small absorbers (typically a fraction

of a square mm). The choice of material involves various trade-offs. Silicon has a low thermal capacity and has been used in early devices, but its drawback is that roughly one-third of the absorbed energy does not end up as heat on a useful time scale but goes into forming electron-hole pairs which, in the absence of any drift bias to sweep them free, become trapped at impurity sites and imperfections in the crystal lattice. The energy resolution then becomes dominated by statistical fluctuations in the fraction of energy converted to heat within the integration time of the detector. The ultimate energy resolution with a silicon absorber used in this manner is then not that given by the above ideal case formula but in fact only twice as good as that of the silicon semiconductor detector. Investigating other materials, we note that insulators, in general, can be treated as wide band semiconductors with the same attendant problems in conversions of energy to heat. Metals, on the other hand, are very good thermalizers, but have the drawback that they have extremely large heat capacity at low temperatures and so could only be used for very small detectors. To date the most promising classes of material are zero bandgap semiconductors and semi-metals, and also superconductors. Among the former, mercuric telluride (HgTe) looks particularly interesting. This material exhibits little or no energy trapping and has returned the best measured results to date as an absorber for single photon calorimeters.

The basic requirement of the thermometer is that it must accurately measure the temperature rise of the absorber with minimal disturbance of the system. Doped semiconductors have a long history of usage as thermometers for infrared detectors and their use for single photon calorimeters has many attractive features despite their being resistance devices which dissipate power when being read out. They can be manufactured with high sensitivities (large resistance change for a given temperature increase), they have high impedances which result in essentially negligible readout amplifier noise, and although their specific heat is higher than that of the pure semiconductor, they can be made extremely small by ion implantation of the dopant into small areas of the device. This latter approach also gets around the problem of attaching the thermometer to the detector. To date these are probably the most widely used and best understood types of thermometer for calorimeter readout.

One of the earliest demonstrations of calorimetry of single x-ray photons was by groups at the University of Wisconsin and NASA's Goddard Space Flight Center.[49] Early results with a 0.25 mm x 0.25 mm silicon absorber at 0.3 K gave 270 eV energy resolution,[49] and at the time of writing this has been improved to

7.3 eV FWHM, using a mercuric telluride absorber at 0.1 K.[50] The absorber is bonded to a single slab of silicon which is etched away to form the necessary mechanical support bars and thermal links. Ion implantation of the silicon is used to form both the thermometer and the conductive tracks leading to it.[51]

A spectrometer based on the single photon calorimeter is currently being developed. Originally intended for the AXAF-S mission, the X-Ray Spectrometer (XRS) will be an array of calorimeters of the type discussed above to provide imaging spectroscopy with greater than 90% efficiency up to 10 keV and response out to 20 keV. The projected energy resolution will be around 10 eV, the device will be operated at 65 milliKelvin, and each pixel, of which there will be around 30, will be 1/4 mm^2 in area.

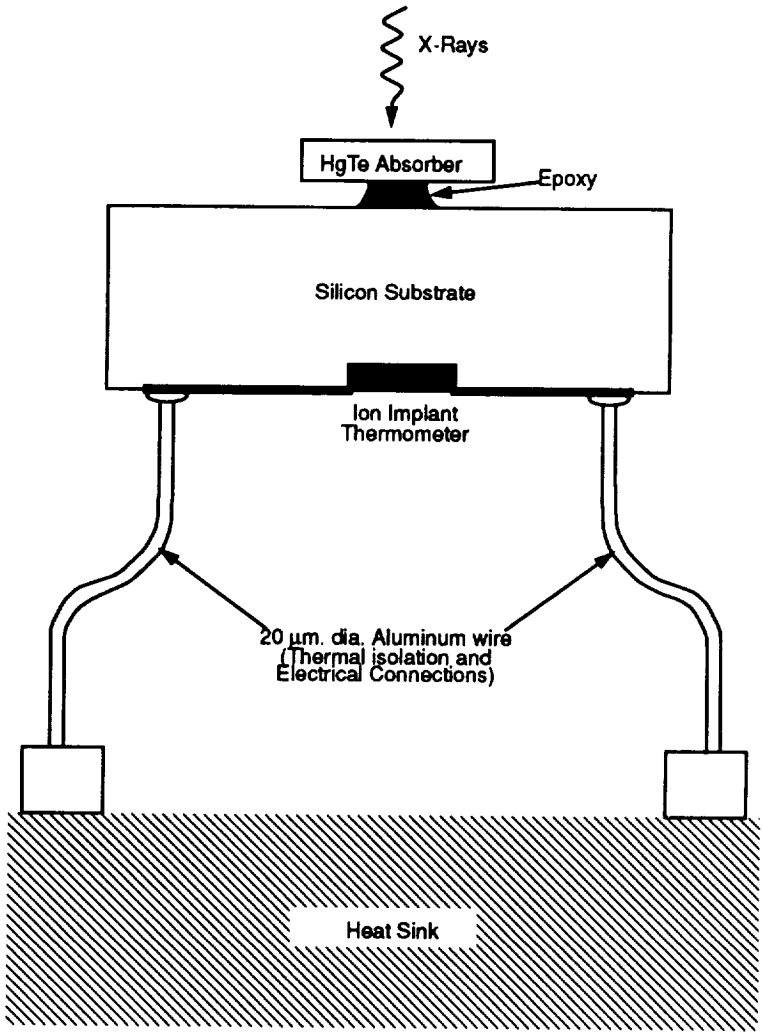

Fig. 26. Construction of a typical calorimeter.

VIII. MISCELLANEOUS DETECTORS

A. LIQUID NOBLE GAS DETECTORS

The gas-filled detectors of section II.A become very inefficient at high energies where the gas becomes transparent to the incident radiation and even at highly elevated pressures (10-20 atm) there is still essentially no sensitivity above a few hundred keV. For operation above this energy a logical extension to the high-pressure chamber is to use the noble gas in liquid form where its density is hundreds of times higher than the gas at atmospheric pressure. Such a detector extends the energy range into the MeV region where Compton interactions and pair production take place in addition to the (lower energy) photoelectric effect. The use of a liquid also dramatically reduces electron diffusion and electron pathlengths so that much higher spatial resolution is possible than with gas-filled detectors.

Of all the noble gases, liquid xenon offers the most promise as an x-ray or gamma ray detector. In addition to its high density and atomic number, which translates into high detection efficiency, it has high electron mobility, is liquefiable at modest temperatures (~160 K) and has a $W \times F$ product (see section II.A) of only 0.64 implying a limiting energy resolution close to germanium ($W \times F = 0.4$) if operated in ionization mode. In fact, the properties of liquid xenon are such that it can, in theory, be operated in all the modes of the equivalent gaseous detector. Thus as well as ionization chambers, proportional counters and proportional scintillation counters (see section II.A) have all been operated in prototype form.[52]

Early attempts to develop useful liquid noble gas proportional counters, though, were largely unsuccessful. While considerable amplification factors (>1000) were obtained in single wire chambers, the scaling up to large area formats with large numbers of anodes proved too challenging as the combination of ultra-fine anode wires (few micron) and very high voltages, necessary to achieve a sufficient field for amplification to occur, rendered the devices unusable due to constant sparking and electrode breakage.[53] The thrust of recent development for astronomy has therefore been toward liquid ionization chambers in which the liberated charge is simply collected without amplification.[54-56]

A liquid xenon ionization chamber is shown schematically in Figure 27. Charge, liberated by the interaction of photons in the absorption region, drifts under the action of a moderate field into a sense region where it induces signals on orthogonal planes of

coordinate wires. These are then read out by individual amplifiers. In this manner both x and y coordinates of the event are measured. The z component of an event can also be obtained, by making use of the fact that liquid xenon is a good scintillator with a light yield comparable to sodium iodide. By measuring the occurrence time of the primary scintillation ultraviolet light, produced when the incident photon interacts in the liquid volume, and comparing this with the charge arrival time at the sense or collection electrodes, the total drift time of the event can be deduced. Armed with a knowledge of the electron drift velocity then the drift distance, and hence the z position, can be calculated.

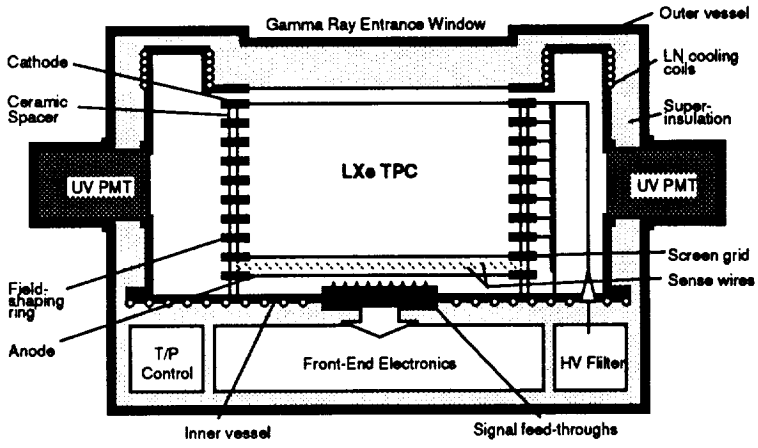

Fig. 27. Cross section of a liquid xenon gamma ray detector (adapted from [56]).

The low-energy response of the liquid ionization chamber is limited by noise in the processing electronics. This is a consequence of the fact that charge multiplication does not take place within the instrument (unlike the proportional counter) and hence the charge signals are necessarily small. A practical low-energy limit would currently seem to be around a few hundred keV. The upper energy limit is once again set by the transparency of the absorbing medium and this will be in the tens of MeV region. Over this operating range the principal interaction mechanisms are Compton scattering and pair production. The former can lead to multiple interactions in the liquid volume which can be fully reconstructed under most circumstances. If the original energy of the photon and its scattering angle can

both be deduced, then the incident direction of the photon can be estimated and a Compton telescope formed. Similarly, if the tracks of the electron/positron pair formed in pair production can be reconstructed, then the initial photon direction can also be estimated. Both modes of operation are capable of giving degree scale angular resolution.

To realize a practical large volume liquid xenon detector for astronomy there are many obstacles to overcome. Among these, the requirement on liquid purity is extremely stringent as the electrons must be drifted to the collection electrodes before they are lost by attachment to impurities. Contaminants must be removed down to the parts per billion level, which is 10^4 times smaller than the tolerance level in gas-filled detectors. Thus sophisticated purification systems must be set up to process the commercially available "high-purity" xenon which has contaminants at the parts per million level and provisions made for keeping the liquid clean over long periods. In addition to attachment to impurities, the newly-liberated electrons may also recombine with xenon atoms before they are drifted away, despite high drift fields, and the fluctuations in this process now appears to be the dominant factor degrading the resolution in current prototype systems.[55]

To date, the liquid xenon chamber is still in its developmental phase and results so far have been taken from small (tens of cm^2) prototype chambers. High spatial resolutions have been achieved with 180 μm rms reported for the resolution in the z direction.[56] Procedures for obtaining the required initial liquid purity are now well developed but the energy resolutions so far reported (6% at 0.57 MeV) are still more than an order of magnitude greater than the Fano limit and this is attributed to the recombination effects outlined above.

X-Ray and Gamma Ray Astronomy Detectors

REFERENCES

1. Petersen, E. L., Instrumental techniques in x-ray astronomy, *Ann. Rev. Astron. and Astrophys.*, 13, 1975.
2. Hillier, R., *Gamma Ray Astronomy*, Clarendon Press, Oxford, 1984.
3. Chupp, E. L., *Gamma Ray Astronomy*, Reidel Publishing Co., Boston, 1976.
4. Ramana Murthy, P. V., and Wolfendale, A.W., *Gamma-Ray Astronomy*, Cambridge University Press, New York, 1986.
5. Knoll, G. F., *Radiation Detection and Measurement*, Second Edition, John Wiley & Sons, New York, 1989.
6. Fraser, G.W., *X-Ray Detectors in X-Ray Astronomy*, Cambridge University Press, New York, 1989.
7. Ramsey, B. D., Austin, R. A., and Decher, R., Instrumentation for x-ray astronomy, *Space Science Reviews*, in press, 1994.
8. Caroli E., Stephen, J. B., Di Cocco, G., Natalucci, L., and Spizzichino, A., Coded aperture imaging in x- and gamma ray astronomy, *Space Science Reviews*, 45, 349, 1987.
9. Wilkinson, D. H., *Ionisation Chambers and Counters*, Cambridge University Press, 1950.
10. Charpak, G., Bouclier, R., Bressani, T., Favier, J., and Zupancic, C., The use of multiwire proportional counters to select and localize charged particles, *Nucl. Instr. and Meth. in Phys. Res.*, 62, 262-268, 1968.
11. Charpak, G., Dominik, W., Santiard, J. C., Sauli, F., and Solomey, N., Gaseous detectors with parallel electrodes and anode mesh planes, *Nucl. Instr. and Meth. in Phys. Res.*, A274, 275-290, 1989.
12. Ramsey, B. D., and Agrawal, P. C., Gas mixtures for x-ray proportional counters, in *SPIE* , vol. 982, pp. 258-264, 1988.
13. Ramsey, B. D., and Agrawal, P. C., Xenon based penning mixtures for proportional counters, *Nucl. Instr. and Meth. in Phys. Res.*, A278, 576-582, 1989.
14. Gaillardetz, R., Bjorkholm, P., Mastronardi, R., Vanderhill, M., and Howland, D., The HEAO-B monitor proportional counter instrument, *IEEE Trans. on Nucl. Sci.*, NS-25(1), 437-444, 1978.
15. Bradt, H. V., Swank, J. H., and Rothschild, R. E., The X-Ray Timing Explorer, *Adv. Space Res.*, 10(2), 297-310, 1990.
16. Turner, M.J.L., Thomas, H. D., Patchett, B. E., Reading, D. H., Makishima, K., Ohashi, T., Dotani, T., Hayashida, K., Inoue, H., Kondo, H., Koyama, K., Mitsuda, K., Ogawara, Y., Takano, S., Awaki, H., Tawara, Y., and Nakamura, N., The large area counter on GINGA, *Publ. Astron. Soc. Japan*, 41, 345-372, 1989.

17. Bateman, J. E., X-ray and gamma imaging with multiwire proportional counters, *Nucl. Instr. and Meth. in Phys. Res.*, 221, 131-141, 1984.
18. Pfeffermann, E., Brial, U. G., Hippmann, H., Kettenring, G., Metzner, G., Predehl, P., Reger, G., Stephan, K. H., Zombeck, M. V., Chappell, J., and Murray, S. S., The focal plane instrumentation of the ROSAT telescope, in *SPIE*, vol. 733, 1986.
19. Ramsey, B. D., and Weisskopf, M. C., The performance of a multistep proportional counter for x-ray astronomy, *IEEE Trans. on Nucl. Sci.*, NS34(3), 672, 1987.
20. Ramsey, B. D., The microstrip proportional counter, in *SPIE*, vol. 1743, pp. 96-103, 1992.
21. Policarpo, A. J.P.L., Alves, M.A.F., Dos Santos, M.C.M., and Carvalho, M.J.T., Improved resolution for low energies with gas proportional scintillation counters, *Nucl. Instr. and Meth. in Phys. Res.*, 102, 337-348, 1972.
22. Simons, D. G., de Korte, P.A.J., Peacock, A., and Bleeker, J.A.M., Energy resolution limitations in a gas scintillation proportional counter, in *SPIE*, vol. 597, pp. 190-198, 1985.
23. Peacock, A., Andresen, R. D., Manzo, G., Taylor, B. G., Villa, G., Re, S., Ives, J. C., and Kellock, S., The gas scintillation proportional counter on EXOSAT, *Space Science Reviews*, 30, 525-534, 1981.
24. Favata, F., and Smith, A., The performance of a low energy gas scintillation proportional counter for the SAX X-Ray Astronomy Satellite, in *SPIE*, vol. 1159, pp. 488-494, 1989.
25. Ohashi, T., Makishima, K., Ishida, M., Tsuru, T., Tashiro, M., Mihara, T., Kohmura, Y., and Inoue, H., Imaging gas scintillation proportional counters for ASTRO-D, in *SPIE*, vol. 1549, pp. 9-19, 1991.
26. Sadoulet, B., Edberg, T. K., Weiss, S., Parsons, A., Wilkerson, J., Hurley, K., Lin, R. P., and Smith, G., High pressure gas scintillation drift chambers with waveshifter readout, in *SPIE*, vol. 1159, pp. 45-56, 1989.
27. Kanbach, G., et al., The project EGRET (Energetic Gamma Ray Experiment Telescope) on NASA's Gamma Ray Observatory, *Space Science Reviews*, 49, 69-84, 1988.
28. Thompson, D. J., et al., Calibration of the Energetic Gamma Ray Experiment Telescope (EGRET) for the Gamma Ray Observatory, *Astrophys. J. Suppl..*, 86(2), 629, 1993.
29. Heath, R. L., Hofstadter, R., and Hughes, E. B., Inorganic scintillators, *Nucl. Instr. and Meth. in Phys. Res.*, 165, 431, 1979.

References

30. Carter, J. N., et al., A position sensitive detector for a gamma-ray imaging telescope, *Nucl. Instr. and Meth. in Phys. Res.*, 196, 477, 1982.
31. Ryan, J. M., COMPTEL, The Imaging Compton Telescope on the Gamma Ray Observatory, in *Gamma Ray Observatory Science Workshop*, edited by W. Neil Johnson (1989) (held Goddard Space Flight Center, Greenbelt, MD, April 10-12, 1989).
32. Diehl, R., The COMPTEL experiment on the NASA Gamma Ray Observatory, *Space Science Reviews*, 49, 85, 1988.
33. Fishman, G. J., et al., BATSE: The Burst and Transient Source Experiment on the Gamma Ray Observatory, in *Gamma Ray Observatory Science Workshop*, edited by W. Neil Johnson, pp. 2.39-2.50 (1989) (held Goddard Space Flight Center, Greenbelt, MD, April 10-12, 1989).
34. Henry, J. P., Kellogg, E. M., Briel, U. G., Murray, S., Van Speybroeck, L. P., and Bjorkholm, P. J., A high resolution imaging x-ray detector for astronomical measurements, in *SPIE*, vol. 106, pp. 196-204, 1977.
35. de Korte, P. A. J., Bleeker, J. A. M., den Boggende, A. J. F., Branduardi-Raymont, G., Brinkman, A. C., Culhane, J. L., Gronenschild, E. H.B.M., Mason, I., and McKechnie, S. P., The x-ray imaging telescopes on EXOSAT, *Space Science Reviews*, 30, 495, 1981.
36. Murray, S. S., Chappell, J. H., Elvis, M. S., Forman, W. R., Grindlay, J. E., Harnden, F. R., Jones, C. F., Maccacaro, T., Tananbaum, H. D., Vaiana, G. S., Pounds, K. A., Fraser, G. W., and Henry, J. P., The AXAF high resolution camera (HRC) and its use for observations of distant clusters of galaxies, *Astro. Lett. and Communications*, 26, 113-125, 1987.
37. Fraser, G. W., Pearson, J. F., and Lees, J. E., Caesium bromide x-ray photocathodes, *Nucl. Instr. and Meth. in Phys. Res.*, A256, 410, 1987.
38. Rossington, C. S., Giauque, R. D., and Jaklevic, J. M., A direct comparison of Ge and Si(Li) detectors in the 2-20 keV range, *IEEE Trans. on Nucl. Sci.*, NS-39(4), 570, 1992.
39. Dabrowski, A. J., et al., Progress in energy resolution of mercuric iodide (HgI_2) x-ray spectrometers, *Nucl. Instr. and Meth. in Phys. Res.*, 213, 89, 1983.
40. Ogawara, Y., et al., X-ray observations of the 1980 Cygnus X-1 'high state,' *Nature*, 295, 675, 1982.
41. Vallerga, J. V., et al., A Bismuth Germanate-shielded mercuric iodide x-ray detector for space applications, *IEEE Trans. on Nucl. Sci.*, NS-29(1), 151, 1982.
42. Serlemitsos, P. J., et al., Broad band x-ray astronomical spectroscopy, *IEEE Trans. Nucl. Sci.*, NS-31(1), 786, 1984.

43. Tueller, J., Observations of gamma-ray profiles from SN 1987A, *Ap. J. Lett.*, 351, L41, 1990.
44. Gehrels, N., Background suppression techniques in germanium detectors, presented at Symposium on Photon Detectors in Space, ESTEC, November 10-12, 1992.
45. Casali, F., et al., Characterization of small CdTe detectors to be used for linear and matrix arrays, *IEEE Trans. Nucl. Sci.*, NS-9(4), 598, 1992.
46. Sze, M., *Semiconductor Devices, Physics and Technology*, Wiley & Sons, Inc., New York, 1985.
47. Garmire, G. P., et al., Performance characteristics of CCD's for the ACIS experiment, in *X-Ray in Astronomy II, SPIE*, vol. 82, pp. 123-128, 1988.
48. Garmire, G. P., et al., The AXAF CCD imaging spectrometer, *AIAA Conference* No. 92, p. 1473, 1991.
49. McCammon, D., Moseley, S. H., Mather, J. C., and Mushotzky, R. F., Thermal detectors as x-ray spectrometers, *J. Appl. Phys.*, 56, 1263, 1984.
50. McCammon, D., Cui, W., Juda, M., Morgenthaler, J., Zhang, R., Kelley, R. L., Holt, S. S., Madjeski, G. M., Moseley, S. H., and Szymkowiak, A. E., Thermal calorimeters for high resolution x-ray spectroscopy, *Proc. 6th European Symposium on Semiconductor Detectors*, Milan, February 1992.
51. McCammon, D., Juda, M., Zhang, J., Holt, S. S., Kelley, R. L., Moseley, S. H., and Szymkowiak, A. E., Thermal detectors for high resolution spectroscopy, *Jap. J. of Appl. Phys.*, 26, 2084-2091, 1987.
52. Incicchitti, A., Belli, P., and Scafi, M., Liquid xenon as a detection medium, *Nucl. Instr. and Meth. in Phys. Res.*, A289, 236-242, 1990.
53. Derenzo, S. E., Schwemin, A., Smits, R. G., Zaklad, H., and Alvarez, L. W., High resolution liquid-filled multi-wire chambers for use in high energy beams, presented at the International Conference on Instrumentation for High Energy Physics, Frascatti, Italy, 1973, Lawrence Berkeley Laboratory Preprint LBL 1791, 1972.
54. Aprile, E., and Suzuki, M., Development of liquid xenon detectors for gamma ray astronomy, Columbia Astrophysical Laboratory Preprint CAL 366, 1988.
55. Aprile, E., Bolotnikov, A., Chen, D., and Mukherjee, R., Liquid xenon time projection chamber for gamma rays in the MeV region: Development status, *SPIE*, vol. 1734, p. 98, 1992.

References

56. Aprile, E., Mukherjee, R., Chan, D., and Bolotnikov, A., A liquid xenon imaging telescope for gamma ray astrophysics: Design and expected performance, Columbia Astrophysical Laboratory Preprint CAL 506, 1992.

INDEX

X-Ray and Gamma Ray Astronomy Detectors

☆U.S. GOVERNMENT PRINTING OFFICE 1994—533-108/00111